

# Natural Fractures in a UK Shale Reservoir Analogue, Cleveland Basin, NE England

Jonathan Imber<sup>1</sup>, Howard Armstrong<sup>1</sup>, Sarah Clancy<sup>1</sup>, Susan Daniels<sup>2</sup>, Liam Herringshaw<sup>1</sup>,  
Ken McCaffrey<sup>1</sup>, Joel Rodrigues, João Trabucho-Alexandre<sup>1</sup>, Cassandra Warren<sup>1</sup>

<sup>1</sup>CeREES Centre for Geoenergy and Durham Energy Institute, Department of Earth  
Sciences, Durham University, Durham, DH1 3LE, UK.

<sup>2</sup>Geospatial Research Ltd., Department of Earth Sciences, Durham University, DH1 3LE,  
UK.

Email: [jonathan.imber@durham.ac.uk](mailto:jonathan.imber@durham.ac.uk)

## Acknowledgements

We are grateful to the Durham Energy Institute, One NorthEast, the Engineering and Physical Sciences Research Council (grant reference EP/J501323/1), the Natural Environment Research Council (grant reference NE/L008092/1) and Geospatial Research Ltd. for funding this study. JI is supported by a Royal Society Industry Fellowship in conjunction with Badley Geoscience Ltd. and Geospatial Research Ltd. (grant reference IF120038). Badley Geoscience Ltd. kindly provided an academic TrapTester license to carry out the elastic dislocation (ED) modelling. Neil Goult and Jon Trevelyan generously shared their knowledge of reservoir geomechanics and fracture propagation. Alex Finlay provided advice on interpreting geochemical proxies, and Graham Yielding commented on the ED modelling results. We are grateful to the AAPG Editors, David A. Ferrill and Michael L. Sweet, for their guidance. Richard H. Groshong, David E. Haddad, Gary G. Lash and Jack C. Pashin provided constructive reviews that challenged our interpretations

and improved our arguments.

### **Abstract (250 words)**

Faults and fractures within the well-exposed Lower Jurassic Cleveland Ironstone and Whitby Mudstone formations may provide insights into the tectonic history of gas-prospective, Mississippian shale in northern England. Sub-vertical opening mode fractures occur throughout the Cleveland Basin. Bed-parallel fractures, some of which contain blocky calcite fills, occur preferentially within well-bedded, clay-rich mudstones of the Cleveland Ironstone and Whitby Mudstone formations at Jet Wyke and Port Mulgrave. Sub-vertical fractures display abutting or curving-parallel relationships with under- and overlying bed-parallel fractures. Together, these observations suggest that bed-parallel fractures, at times, acted as free surfaces. Some bed-parallel fractures curve towards and branch from calcite-filled fault slip surfaces, indicating that bed-parallel fracturing and normal faulting were synchronous, occurring within a regional stress field with vertical maximum principal stress. This apparent paradox can be explained by normal compaction, followed by cementation and coupling between pore pressure and minimum horizontal stress driven by poroelastic deformation or incipient slip along critically stressed normal faults, causing elevation of horizontal stress in excess of the vertical stress within clay-rich units. Propagation of bed-parallel fractures was enhanced by dilatational strains adjacent to normal fault planes. Bed-parallel fractures have not been observed within more SiO<sub>2</sub>-rich units at the top of the Whitby Mudstone Formation at Whitby East Cliff, or within well-bedded, clay-rich shale at Saltwick Nab. This observation is consistent with the lack of normal faulting at Saltwick Nab, and the Whitby Mudstone Formation having been drained by structural and/or stratigraphical juxtaposition against permeable Middle Jurassic sandstones at both these localities.

## Introduction

Shale gas exploration in the UK is in its infancy. The British Geological Survey has recently produced a resource estimate for the Carboniferous (Mississippian) Bowland-Hodder shale unit in northern England, with total gas-in-place estimates of 822 (P90), 1329 (P50) and 2281 (P10) trillion cubic feet (Andrews, 2013). However, there are insufficient data to yet estimate the recovery factor or potential reserves.

US experience has shown that natural fractures are important for producing shale gas. Natural fractures, bedding planes and minor faults may reopen or reactivate during hydraulic stimulation, so understanding the geometry of natural fracture systems, and the relationship between natural fractures and minor faults, is important for efficient design of hydraulic fracture treatments and optimising recovery (e.g. Gale et al., 2007; Thiercelin and Makkhyu, 2007; Warpinski et al., 2009; Zoback et al., 2012).

Fault and fracture data from the Bowland-Hodder shale unit are limited within the prospective area covered by the Andrews (2013) assessment, owing to the low density of wells, limited availability of 3D seismic reflection data, and generally poor exposure where the Bowland-Hodder shale unit occurs at outcrop. The aim of this study is to investigate the nature and distribution of burial-related natural fractures within the better-exposed Lower Jurassic Cleveland Ironstone (Pliensbachian) and Whitby Mudstone (Toarcian) formations of the Cleveland Basin, NE England (Figs 1, 2 and 3). Part of the Cleveland Basin overlies a Carboniferous (Mississippian) depocentre (Fraser and Gawthorpe, 2003), which locally contains > 3000 m of Bowland-Hodder shale unit (fig. 18 of Andrews, 2013). Structural studies of the Cleveland Ironstone and Whitby Mudstone formations may provide insight into the processes that controlled the post-Triassic tectonic history and fracturing of the Bowland-Hodder shale unit in NE England. Our specific objectives are to evaluate the controls of (1) lithostratigraphic variability, (2) regional variations in burial, diagenetic and tectonic histories, and (3) the occurrence of minor faults on natural fracture

development within the Cleveland Basin. This study draws extensively upon an existing body of research into naturally fractured black shales in US shale gas basins (e.g. Lash and Engelder, 2005; Gale et al., 2007; Engelder et al., 2009; Pashin et al., 2012).

The Cleveland Ironstone and Whitby Mudstone formations are well exposed in cliff sections and on clean, wave-washed platforms along the North Yorkshire coast (Fig. 1; Rawson and Wright, 2000). Importantly, a litho- and chronostratigraphic framework in which to understand fault and fracture evolution has already been established (Howarth, 1955, 1962; Powell, 1984; Rawson and Wright, 1996; Cox et al., 1999; Powell, 2010). The Whitby Mudstone Formation includes the “Jet rock” (an informal, lithostratigraphic division; Fig. 3), with total organic carbon (TOC) content that locally exceeds 18 % (e.g. McArthur et al., 2008). The Cleveland Ironstone and Whitby Mudstone formations also contain leaner intervals characterised by variable quartz, carbonate and clay contents. Prior to exhumation, the Whitby Mudstone Formation and, by inference, the underlying Cleveland Ironstone Formation was buried to the early oil window (Williams, 1986; Sælen et al., 2000; Kemp et al., 2005; French et al., 2014). The Cleveland Ironstone and Whitby Mudstone formations may therefore provide useful analogues to help understand structural processes operating within prospective self-sourced shale reservoirs elsewhere in the UK, including the Bowland-Hodder shale unit in northern England (Andrews, 2013), and the Lower Jurassic (Liassic) shale of the Weald Basin, SE England (Department of Trade and Industry, 2003, p. 42).

We start by defining key terms and summarising the geological history of the Cleveland Basin. We then describe the lithostratigraphy of the Cleveland Ironstone and Whitby Mudstone formations, and present observations of faults and fractures within the Cleveland Ironstone Formation at Jet Wyke, and the Whitby Mudstone Formation at Port Mulgrave, Whitby East Cliff and Saltwick Nab. Together, these localities lie along a discontinuous, ca. 15 km long coastal transect (Fig. 1). By way of comparison, UK

Petroleum Exploration and Development Licence (PEDL) 165, which includes part of the prospective Bowland-Hodder shale unit resource in northern England, covers an area of ca. 30 x 40 km (Department of Energy and Climate Change, 2014). Our findings suggest that fracture patterns in UK shale basins are likely to be heterogeneous over distances < 15 km, i.e. on a scale smaller than some existing UK shale gas exploration licences. We suggest that these spatial and stratigraphic variations are effectively unpredictable in the absence of detailed knowledge of the lithostratigraphy, and burial, diagenetic and tectonic histories across the license area.

## Definitions and approach

Throughout this study, we take “fracture” to mean a vein or joint, i.e. an opening-mode discontinuity with or without mineral fill. “Shear fracture” denotes a structure characterised by measurable shear displacement across its boundaries, but lacking well-developed fault rock. A “fault” is defined as a structure with measurable shear displacement across its boundaries, which contains fault rock. Where possible, we establish the relative ages of different fracture sets based on observed abutting and cross-cutting relationships (Dyer, 1988; Engelder, 1993). At the Whitby East Cliff locality, we are able to place broad limits on the absolute timing of fracture growth by analyzing the cross-cutting relationships between the dominant fracture sets and the region-wide Middle Jurassic (Aalenian) unconformity (see below). However, recognizing the difficulty in correlating fracture sets on a regional basis (see discussion in Engelder, 1993, p. 53-56), we further attempt to use cross-cutting and/or branching relationships to define the relative ages of fracture sets with respect to minor faults observed at Jet Wyke, Port Mulgrave and Whitby East Cliff. Underlying this approach is the assumption that the minor faults formed during recognisable tectonic events and the type of faulting (i.e. normal, reverse, strike-slip) reflects the orientation of the principal stresses at the time of slip (Anderson, 1951, cf.

Addis et al., 1996). Other terms used within this paper are listed and defined in Table 1.

## Geological Setting of the Cleveland Basin

### Burial and tectonic subsidence

The Cleveland Basin was an important Jurassic depocentre linked via the Sole Pit Basin to the North Sea Basin (Ziegler, 1982). It was bounded to the south by the Market Weighton High, and to the north and west by the Mid North Sea and Pennine Highs, respectively. Eroded remnants of this Jurassic depocentre crop out in NE England (Fig. 2a).

Fraser and Gawthorpe (2003) recognised a phase of Mississippian rifting in northern England. Backstripped (water loaded) tectonic subsidence curves derived from onshore borehole data from across the Cleveland Basin (Fig. 2b; Dixon, 1989) display < 800 m rapid tectonic subsidence during latest Permian to earliest Triassic times, followed by decreasing rates of tectonic subsidence throughout the Mesozoic. Dixon (1989) argued that these tectonic subsidence curves are consistent with major, late Permian to earliest Triassic rifting, followed by thermal subsidence. The shape of the curves is consistent with a stretching factor ( $\beta$ ) between 1.2 and 1.25, assuming instantaneous, uniform stretching (Dixon, 1989).

Despite the generally decreasing rate of tectonic subsidence throughout the Mesozoic, data obtained from the Fordon 1 and Staithes 4 boreholes highlight three periods of more rapid subsidence (< 300 m) that took place during the Early Jurassic, Late Jurassic and Cretaceous (arrows, Fig. 2b). These periods may have been associated with active faulting within and along the margins of the Cleveland Basin. Nevertheless, average burial rates remained low (< 20 m Myr<sup>-1</sup>) throughout Late Jurassic to Palaeogene times (e.g. see fig. 12 of Williams, 1986).

Local tectonic activity, including movements on N-S to NNW-SSE striking normal faults

(Runswick Bay fault, Whitby Harbour fault, Peak fault; Fig. 2a) in the vicinity of our study area took place during Early, Middle and Late Jurassic to Early Cretaceous times (Milsom and Rawson, 1989). Field relationships (Howarth, 1962; Alexander, 1986; Alexander and Gawthorpe, 1993) and interpretations of seismic reflection profiles (Milsom and Rawson, 1989) demonstrate that changes in sediment thickness and/or facies take place across these faults within the Lower Jurassic Whitby Mudstone and Middle Jurassic Saltwick formations. These observations suggest that movements on the Runswick Bay, Whitby Harbour and Peak faults were, at least in part, syn-sedimentary and led to subtle, localised topographic expressions during the Early and Middle Jurassic epochs. It is not clear whether these syn-sedimentary normal faults are thin-skinned, or the upward continuation of Carboniferous “basement” or Late Permian faults (cf. Fraser and Gawthorpe, 2003). For example, seismic reflection profiles presented by Milsom and Rawson (1989) suggest that the Peak fault – the largest Jurassic syn-sedimentary fault exposed within the Cleveland Basin – detaches on the underlying Triassic shales and Zechstein (Permian) evaporites. In summary, we infer tectonic subsidence during deposition of the Lower Jurassic Cleveland Ironstone and Whitby Mudstone formations was primarily controlled by thermal re-equilibration following late Palaeozoic to early Triassic rifting, locally modified by displacements along N-S to NNW-SSE striking syn-sedimentary normal faults. Such a tectonic environment is likely to have been characterised, at least on a regional scale, by vertical maximum principal stress, i.e.  $S_v = \sigma_1$  (Table 1).

### **Exhumation and inversion**

The Jurassic succession within the Cleveland Basin is cut by a number of unconformities. The key unconformity surface for the purposes of this study is that which separates the Lower Jurassic Whitby Mudstone Formation from the Middle Jurassic (Aalenian) Dogger

and Saltwick formations (Fig. 3). The Lower Jurassic succession is thickest in the east (i.e. along the coast) and thins regionally southward onto the Market Weighton block, a long-lived paleo-high in the footwall of the Flamborough fault zone (Figs 2a, c). The Lower Jurassic also thins locally along the coast, between Whitby and Ravenscar (Fig. 2c). This local thinning can, at least in part, be attributed to ca. 60 m uplift and erosion of the (then) still poorly lithified sediments comprising the uppermost Whitby Mudstone Formation during latest Toarcian to earliest Aalenian times (Powell, 2010). At the same time, uplift in the western part of the basin led to exhumation of deeper stratigraphic levels within the Whitby Mudstone Formation (Grey Shale Member). This variability in intra-Jurassic burial and exhumation histories has implications for understanding natural fracture development across the Cleveland Basin, as discussed below.

The Jurassic rocks within the Cleveland Basin reached their maximum burial depth during latest Cretaceous to earliest Paleogene (Williams, 1986; Green, 1989; Bray et al., 1992) or Oligo-Miocene (Holliday, 1999) times. The presence of mixed layer clays, which contain 90% illite within Lower Jurassic mudstones, suggests a maximum burial depth of ca. 4 km (Kemp et al., 2005). The basin was subsequently inverted, producing the broadly E-W trending Cleveland anticline, and associated minor fold structures (Hemingway and Riddler, 1982; Fig. 2a). The precise timing of inversion is uncertain, but occurred sometime between the latest Cretaceous to Neogene (Powell, 2010). Tectonic inversion is likely to have been characterised, at least on a regional scale, by vertical minimum principal stress, i.e.  $S_v = \sigma_3$  (Table 1).

## **Lithostratigraphy of the Cleveland Ironstone and Whitby Mudstone Formations**

The Pliensbachian Cleveland Ironstone Formation is ca. 25 m thick (Powell 2010) and

crops out on the coast between Staithes and Brackenberry Wyke (Fig. 1; 0.7876°W, 54.5593°N to 0.7739°W, 54.5537°N (decimal longitude and latitude, WGS84)). According to Macquaker and Taylor (1996), the Cleveland Ironstone Formation comprises four distinct lithofacies: clay-rich mudstones, silt-rich mudstones, sand-rich mudstones and concretionary carbonates (the latter include the eponymous sideritic ironstone horizons). These lithological units stack to form small-scale upward-coarsening packages (0.1 to 1 m thick). Upward-coarsening and upward-fining packages are also recognised on a larger (1 to 3 m) scale (Macquaker and Taylor, 1996; Fig. 3, inset). The mean ratio of (silt+sand+carbonate+shell fragments) to (silt+sand+carbonate+shell fragments+clay) is 3.9%, 13%, 31% and 76% in clay-rich, silt-rich and sand-rich mudstone, and concretionary carbonate, respectively (Macquaker and Taylor, 1996; Fig. 3, inset). By contrast, total organic carbon (TOC) is uniformly low, with mean values of 0.7%, 0.91% and 0.75% in the clay-rich, silt-rich and sand-rich mudstones, respectively (Taylor and Macquaker, 2000; Fig. 3).

The Toarcian Whitby Mudstone Formation is ca. 70 m thick (< ca. 105 m thick in the hanging wall of the syn-sedimentary Peak fault; Fig. 2a) and crops out along the coast between Blackenberry Wyke and Sandsend (-0.7739°W, 54.5537°N to 0.6719°W, 54.5050°N), and Whitby East Cliff to White Stone Hole (0.6105°W, 54.4917°N to 0.5346°W, 54.4567°N). For our purposes, it is useful to divide the Whitby Mudstone Formation into 6 informal lithostratigraphic units, based on Howarth's (1962) detailed lithostratigraphic and palaeontological analysis (oldest to youngest; Fig. 3): Grey shale (corresponding to the Grey Shale Member of the Whitby Mudstone Formation; Fig. 3), Jet rock and Bituminous shale (corresponding to the Mulgrave Shale Member of the Whitby Mudstone Formation), and Hard shale, Main Alum shale and Cement shale (corresponding to the Alum Shale Member of the Whitby Mudstone Formation). We focus on the Jet rock, Bituminous shale and Cement shale intervals.

The Jet rock (ca. 7.5 m thick) and overlying Bituminous shale (ca. 23 m thick) comprise thinly-bedded mudstone and siltstone layers (beds typically < 2 cm thick). These layers define small-scale fining upward sequences (< 5 cm thick), with evidence for scouring at the base of silty layers. The Jet rock contains abundant diagenetic carbonate concretions (e.g. Raiswell, 1976, 1982; Raiswell and White, 1978) and is capped by a laterally continuous carbonate bed with abundant coccoliths (Sælen et al., 2000; “Top Jet dogger”; Fig. 3) (“dogger” is an historical ironstone mining term that refers to hard carbonate beds or concretions). Bedding planes appear to bend around individual concretions, an observation which suggests that the concretions formed prior to lithification of the Jet rock, probably within 3 m of the palaeo-sea floor (Raiswell, 1976). Other evidence for early cementation and breaks in sedimentation within the Jet rock include the presence of mineralised biofilms (< 0.5 cm thick) and authigenic dolomite rhombs (Pye and Krinsley, 1986). Early-formed carbonate concretions are also present in the Bituminous shale, but are smaller and less abundant than in the Jet rock (Fig. 3).

The Jet rock has a mean TOC of 6.5%, reaching a maximum of 18.2% within beds 35-36 (McArthur et al., 2008, following Howarth's, 1962 bed numbering scheme; Fig. 3). By contrast, SiO<sub>2</sub>, Al<sub>2</sub>O<sub>3</sub> and K<sub>2</sub>O all decrease to minima of 32 weight (wt) %, 11 wt% and 2 wt%, respectively, within this stratigraphic interval (Pye and Krinsley, 1986; Fig. 3). These minima reflect the relatively high concentration of organic material, and correspondingly lower concentrations of detrital quartz and clay. The SiO<sub>2</sub>/Al<sub>2</sub>O<sub>3</sub> ratio, however, reaches a local maximum (2.9) within the Jet rock (Pye and Krinsley 1986; Fig. 3). The increase in the SiO<sub>2</sub>/Al<sub>2</sub>O<sub>3</sub> ratio could be caused by enhanced input of either biogenic silica or terrigenous quartz, or decreased input of clay. Zr is associated with the heavy mineral zircon, and is a proxy for silt-sized terrestrial input into the basin (Ratcliffe et al., 2012). There is a positive correlation between SiO<sub>2</sub> and Zr (n = 21, r = 0.758) within the Whitby Mudstone Formation (Fig. 3), implying that the increase in SiO<sub>2</sub>/Al<sub>2</sub>O<sub>3</sub> ratio is consistent

with increased input of detrital quartz during deposition of the Jet rock. This interpretation is consistent with the lack of petrographic evidence for biogenic silica within this interval. The abundance of CaO is high, but variable (4.1 wt% to 7.4 wt%; Fig. 3).

The Bituminous shale has a mean TOC of 3.1%, with the highest value (4.6%) recorded in the interval directly above the Jet rock (McArthur, et al. 2008; Fig. 3). SiO<sub>2</sub>, Al<sub>2</sub>O<sub>3</sub> and K<sub>2</sub>O are typically higher in the Bituminous shale than in the Jet rock, and have mean values of 47 wt%, 21 wt% and 3.2 wt%, respectively. CaO has a mean abundance of 3.1 wt%. The SiO<sub>2</sub>/Al<sub>2</sub>O<sub>3</sub> ratio has a maximum value of nearly 2.5 directly above the Top Jet dogger, but decreases upwards, reaching a near-constant value of ca. 2.1 (Pye and Krinsley, 1986; Fig. 3). This observation suggests that clastic input during deposition of the Bituminous shale may have been dominated by clay minerals, rather than quartz.

Based on quantitative mineralogical data presented by Kemp et al. (2005) and Jeans (2006), the ratio of (quartz+carbonate) to (quartz+carbonate+clay) within the Jet rock and Bituminous shale varies from 27% to 33% (Fig. 3). According to Gad et al. (1968), the proportions of sand (> 50 µm), silt (2 to 50 µm) and clay (< 2 µm) particles in the Jet rock are 0.01%, 48.0% and 52.0%, respectively. The corresponding proportions within the Bituminous shale are 0.1%, 44.7% and 55.2%, respectively.

Kemp et al. (2011) presented high-resolution organic carbon, sulphur and carbonate concentration data for two intervals (beds 21 to 34 and 41 to 43; Fig. 3) within the Grey Shale, Jet rock and Bituminous shale. These authors conducted spectral analysis and identified regular cyclicity in CaCO<sub>3</sub>, TOC and S (sulphur) with a wavelength of ca. 60 cm within the lowermost part of the Bituminous shale (corresponding approximately to Howarth's (1962) beds 41 to 43; Fig. 3). An additional spectral peak is also present in CaCO<sub>3</sub> and S with a wavelength of ca. 112 cm. Kemp et al. (2005, 2011) argued that the observed cyclicity was controlled by astronomical forcing (e.g. obliquity or precession). As such, the cyclicity observed in CaCO<sub>3</sub>, TOC and S may reflect cyclic changes in the

broader mineralogy and sedimentology of the Bituminous shale, a point we return to below.

Outside the Peak Trough (a NNW-SSE striking graben bounded by the syn-sedimentary Peak fault; Milsom and Rawson, 1989), the Cement shale (ca. 6 m thick) marks the top of the Whitby Mudstone Formation and lies directly below the unconformable Middle Jurassic (Aalenian) Dogger and Saltwick formations. In contrast to the Jet rock and Bituminous shale, bedding within the Cement shale is poorly defined, possibly as a result of bioturbation. Macroscopic trace fossils are observed from Bed 53 of the Main Alum shale upwards, and pyritized burrows are common in the Cement shale. The Cement shale contains numerous diagenetic carbonate concretions (Fig. 3) that occur within irregular layers, and dispersed throughout the rock matrix. The Cement shale has a mean TOC of 1.2 % (McArthur et al., 2008) and mean values of SiO<sub>2</sub>, Al<sub>2</sub>O<sub>3</sub>, K<sub>2</sub>O and CaO of 54 wt %, 22 wt %, 3.1 wt % and 0.42 wt %, respectively. The mean SiO<sub>2</sub>/Al<sub>2</sub>O<sub>3</sub> ratio is 2.4 (Pye and Krinsley, 1986; Fig. 3), suggesting greater input of quartz and lower input of clay minerals into the basin during deposition of the Cement shale, compared with the underlying Bituminous shale. Quantitative mineralogical data for the Cement shale are limited, but the ratio of (quartz+carbonate) to (quartz+carbonate+clay) is around 32 % (Kemp et al., 2005; Fig. 3). According to Gad et al. (1968), the proportions of sand (> 50 µm), silt (2 to 50 µm) and clay (< 2 µm) particles in the Cement shale are 1.5 %, 45.0 % and 53.5 %, respectively.

## Summary of basin history and lithostratigraphy

This review of the lithostratigraphy and burial, inversion and exhumation histories highlights three points. First, the variable abundances of quartz, carbonate, clay and TOC suggest that the elastic properties of the Cleveland Ironstone and Whitby Mudstone formations are unlikely to be homogeneous (cf. Rickman et al., 2008; Aoudia et al., 2010).

Second, the well-developed bedding in the Cleveland Ironstone Formation, Jet rock and Bituminous shale, but not the Cement shale, suggests that the former, but not the latter, are likely to display anisotropic tensile strength. Third, the regional differences in burial, exhumation and diagenetic histories suggest that otherwise similar lithostratigraphic units may have followed different stress paths in different parts of the basin (e.g. Mayne and Kulhawy, 1982; Jones, 1994; Goult, 2003). All these factors are likely to influence the style and abundance of natural fractures.

Ideally, we would follow a quasi-experimental approach to investigate how each factor (e.g. development of bedding) in turn influences the style of deformation, with all other factors (e.g.  $\text{SiO}_2/\text{Al}_2\text{O}_3$  ratio, etc.) being constant. Unfortunately, the available outcrop means we are restricted in the number of possible comparisons, and can only draw qualitative inferences on the importance of each factor in controlling faulting and fracturing. A further limitation is that we focus on natural fractures that we can reasonably infer to have developed during burial, prior to exhumation. Excluding possible inversion-related structures obviously ignores an important part of the structural evolution, but removes uncertainty that could impede generic understanding of processes that may have controlled fracture development in the Cleveland Basin. The studied outcrops, and their key lithological, geochemical and structural characteristics are summarised in Figure 1 and Table 2.

## **Faults and Fractures in the Cleveland Basin**

### **Cleveland Ironstone Formation at Jet Wyke**

We focus on faults and fractures within the interval between the Osmotherley and Raisdale (ironstone) seams (Fig. 3), the upper part of which was studied in detail by Macquaker and Taylor (1996). At Jet Wyke, the Cleveland Ironstone Formation dips gently towards the

east, and is cut by segmented, N-S to NNW-SSE striking faults. These faults display apparent normal separations, with throws typically in the range 1 m to 5 m (Fig. 4a). The largest faults dip towards the W at 40° to 60°, and are associated with zones of shale gouge and breccia, up to 1 m thick. Where present, slickenlines (grooves) on slip surfaces at the edge of gouge zones consistently plunge down-dip. We infer that normal faulting probably occurred during basin subsidence, at a time when the regional stress field was characterised by  $S_v = \sigma_1$ . However, there is no evidence at Jet Wyke for across-fault changes in sediment thickness or facies, indicating that the faults exposed on the foreshore initiated after deposition of the Cleveland Ironstone Formation.

Two swarms of bed-parallel veins, with blocky calcite fills, give rise to distinct erosive notches in cliff sections (white arrows in Fig. 4a). These notches can be traced for ca. 400 m around Jet Wyke, and maintain near-constant stratigraphic height – ca. 2.7 m and 1.2 m below the base of the Avicula Ironstone Seam and Raisdale seam (Fig. 3), respectively – within each fault-bounded block. Comparison with Macquaker's and Taylor's (1996) detailed lithostratigraphic data shows that the bed-parallel veins beneath the Raisdale seam occur where the (sand+silt) to clay ratio  $< 0.2$  (Fig. 3, inset), i.e. within clay-rich parts of the succession. Mineralogical ratios are not available for the interval between the Osmotherley seam and Avicula Ironstone Seam, but it is apparent from field observations and the published lithological log of the Cleveland Ironstone Formation (Rawson and Wright, 2000; Fig. 3) that the bed-parallel veins beneath the Avicula Ironstone Seam also occur within a clay-rich interval.

In detail, notches contain single or multiple (Fig. 4b) bed-parallel veins. The continuity of individual bed-parallel veins is variable, and individual veins locally display low-angle discordance to bedding (Fig. 4b). Narrow ( $< 1$  cm thick), laterally discontinuous bands of brecciated shale are occasionally seen along the upper margins of bed-parallel veins. More commonly, irregularities in the vein wall can be matched directly across bed-parallel

vein fills (Fig. 4c), so we infer an opening mode origin with possible minor shear reactivation. The presence of calcite-filled, bed-parallel fractures is consistent with the pore fluid pressure ( $P_p$ ) having been equal to the overburden stress ( $S_v$ ) at the time of fracture opening. This observation appears to contradict our inference that, regionally,  $S_v = \sigma_1$ , and is discussed further below (Analysis).

Sub-vertical fractures, with or without thin calcite fills, abut downwards onto bed-parallel veins (Fig. 4a). Sub-vertical fractures below the Avicula Ironstone Seam are regularly spaced at ca. 1 m intervals, whilst sub-vertical fractures within the Avicula Ironstone Seam itself are more closely, albeit regularly spaced. Fracture surfaces display well-developed plumose markings and elliptical arrest lines, which are consistent with tensile (Mode 1) opening (e.g. Bahat and Engelder, 1984; Fig. 4d). The abutment relationship suggests that the sub-vertical fractures formed whilst the bed-parallel veins remained open.

### **Jet Rock and Bituminous Shale (Whitby Mudstone Formation) at Port Mulgrave**

The exposures at Port Mulgrave lie in the hanging wall of the syn-sedimentary Runswick Bay fault (Fig. 2a), which crops out ca. 900 m to the east of the studied localities, but was poorly exposed at the time of writing. The pattern of faulting is complex (see plate 26 of Howarth, 1962), and appears to comprise two main sets: (1) N-S to NNW-SSE striking faults, parallel or sub-parallel to the Runswick Bay fault; and (2) WNW-ESE striking faults.

The WNW-ESE striking faults dip moderately towards the SW or NE ( $35^\circ$  to  $55^\circ$ ) and are associated with gently pitching calcite slickenfibres (Fig. 5a). The geometries of sigmoidal veins, viewed in surfaces approximately parallel to the slickenfibres and which contain the pole to the fault plane, are consistent with dextral-oblique slip along these WNW-ESE faults. Such dextral-oblique movement can explain the reverse separation (ca. 50 cm) of the Top Jet dogger (bed 39 on Fig. 3) across a prominent WNW-ESE striking fault at

0.7684°W, 54.5462°N.

A ca. 5 m wide fault zone, bounded by two NNW-SSE striking faults is exposed at 0.7673°W, 54.5458°N. The bounding faults dip moderately to steeply (52° to 84°) towards the east or west, and are associated with gently to moderately (8° to 46°) SSE-plunging slickenlines (Fig. 5a). Rotation of beds within the fault zone is consistent with sinistral-oblique slip across the entire zone. Together, the dextral- and sinistral-oblique slip faults appear to form a conjugate set that presumably developed at a time when  $S_v = \sigma_2$ . We infer that these faults were active during latest Cretaceous to Neogene basin inversion; these postulated inversion-related faults and associated minor structures are not considered further here.

The majority of faults at Port Mulgrave strike NNW-SSE and dip moderately (26° to 64°) towards the W or E (Fig. 5b). The faults typically contain poorly consolidated shale gouge (< 1 m thick; Fig. 5c), containing variable abundances of calcite veins. Slip surfaces along the margins of shale gouge layers contain down-dip to steeply pitching grooves or calcite slickenfibres, indicative of dip-slip displacement. Drag of beds adjacent to slip surfaces (Fig. 5c), the presence of calcite- and/or bitumen-stained dilatational jogs along slip surfaces (Fig. 5d), the sense of rotation of carbonate concretions caught up within fault zones (Fig. 5c), and dip separation (ca. 1 m) of distinctive marker beds (e.g. bed 35, Fig. 3; Zijp et al., 2014) are all consistent with normal movement. We therefore infer that such faults developed at a time when  $S_v = \sigma_1$ , most likely during basin subsidence. There is no evidence for across-fault changes in sediment thickness or facies within the Whitby Mudstone Formation at Port Mulgrave, which suggests that these normal faults initiated after deposition of the Jet rock and Bituminous shale sequence.

Fracture patterns within the Jet rock and Bituminous shale at Port Mulgrave are qualitatively similar to those observed within the Cleveland Ironstone Formation at Jet Wyke. The rock volumes surrounding the normal faults contain arrays of bed-parallel and

sub-vertical fractures (Figs 6a, b) with absent to well-developed calcite infills. Bed-parallel fractures appear to be particularly common within the Bituminous shale (Fig. 6c).

It is difficult to correlate bed-parallel fractures across normal faults (similar to Jet Wyke), despite the small, metre to sub-metre scale fault displacements. This observation suggests that bed-parallel fractures did not behave as passive markers and, taken in their entirety, do not pre-date normal faulting. Many individual bed-parallel fractures terminate abruptly against fault slip surfaces, indicating they pre-date the final slip increment. However, calcite-filled bed-parallel fractures in the hanging wall of an ENE-dipping normal fault (0.7682°W, 54.5465°N) curve towards (in a concave-up sense) and merge with the calcite-lined principal slip surface (Fig. 6d). Together, these relationships suggest that the bed-parallel fractures probably formed during the same geological event as the normal faults, i.e. within a regional stress system in which  $S_v = \sigma_1$ . This apparent contradiction is discussed further below.

Within the clay-rich Bituminous shale, bed-parallel fractures are regularly spaced between 70 and 150 cm (Fig. 6c). This range of fracture spacings is comparable to the dominant wavelengths of cyclicity in  $\text{CaCO}_3$ , S (sulphur) and TOC (ca. 60 cm and 112 cm) recorded within the lower part of the Bituminous shale (Kemp et al., 2011). Some gently-dipping fractures are locally discordant to bedding and in places appear to merge with gently-dipping, gouge-lined slip surfaces (Fig. 6c). This observation suggests that at least some bed-parallel fractures have accommodated bed-parallel shear. Nevertheless, many bed-parallel fractures contain blocky, inward-coarsening calcite fills (Fig. 6e; cf. syntaxial veins defined by Bons et al., 2012) with no evidence for shear displacement even where veins are locally discordant to bedding. These textures suggest that many bed-parallel fractures originated as opening mode structures that were held open for sufficient time to allow crystallisation into void spaces.

Sub-vertical fractures abut downwards and upwards onto bed-parallel fractures, an

observation which is consistent with the bed-parallel fractures having provided a free surface, and supports the contention that these fractures were, at times, open. Elsewhere in the same outcrop, sub-vertical fractures curve, in a concave-up sense, as they approach and merge with underlying bed-parallel fractures (Fig. 6f). This curvature could either result from a component of shear stress acting along a (closed) bed-parallel fracture, or from propagation of an initially sub-vertical joint towards an open bed-parallel fracture, assuming the effective crack-parallel stress was compressive, and the effective crack-normal stress ( $S_v$ ) was tensile (Dyer, 1988). Together, our observations likely suggest that the bed-parallel fractures were at times open (acting as free surfaces) and at other times closed (supporting a shear stress), possibly during minor shear reactivation. The presence of open, bed-parallel fractures is consistent with the pore fluid pressure ( $P_p$ ) having been equal to the overburden stress ( $S_v$ ).

### **Cement Shale (Whitby Mudstone Formation) at Whitby East Cliff**

The exposures of Cement shale at Whitby East Cliff (Fig. 2a) lie directly below the uppermost Toarcian to lowermost Aalenian unconformity. The Cement shale is intensely faulted and fractured, and is cut by two main sets of structures: NNW-SSE striking faults and NNW-SSE striking, sub-vertical fractures (Figs 7a, b). Bed-parallel fractures similar to those observed at Jet Wyke and Port Mulgrave have not been observed.

The NNW-SSE striking faults dip between  $5^\circ$  and  $62^\circ$  towards the WSW, and strike parallel to the Whitby Harbour fault (e.g. see fig. 2 of Alexander and Gawthorpe, 1993). Fault traces observed in the vertical cliff section form a linked network (Fig. 7b). The faults contain lenses of brecciated shale (< 2 cm thick) and – locally (see below) – calcite infills. Slickenlines or slickenfibres have not been observed, but faults consistently display normal separations (< 5 cm) where they cut carbonate concretions (Fig. 7b). Nevertheless, layers of carbonate concretions maintain fairly constant heights across the outcrop, which

suggests the overall displacement across the entire fault network (which occupies a zone < 30 m wide) is small. We have not observed any across-fault changes in sediment thickness or facies, which suggests that the faults initiated after deposition of the exposed Cement shale. Similar to Jet Wyke and Port Mulgrave, we infer that normal faulting occurred at a time when the regional stress system was characterised by  $S_v = \sigma_1$ , presumably during basin subsidence.

Sub-vertical fractures contain intensely weathered, yellowish calcite fills and comprise two distinct groups. The first are short, irregular fractures (< 2 m) that branch upwards and downwards from fault surfaces (Fig. 7b). These fractures are ubiquitous throughout the outcrop. Less commonly observed are vertically continuous, albeit segmented fractures (Fig. 7c) that continue across the uppermost Toarcian to lowermost Aalenian unconformity to cut Middle Jurassic sediments of the Dogger and Saltwick formations. This observation suggests that the vertically continuous, sub-vertical fractures post-date deposition of the Saltwick Formation. Shear displacements have not been observed across sub-vertical fractures, which we infer to be opening mode in origin.

In places, the fractures are segmented where they intersect fault surfaces (Fig. 7c). Individual segments terminate against the fault, and calcite mineralisation occurs along fault surfaces less than 10 cm from the intersection. Elsewhere, faults appear to terminate against vertically continuous, sub-vertical fractures. Fault terminations are marked by wide (< 10 cm thick) zones of shale breccia that become narrower away from the point of intersection. We infer that the breccia zones accommodate increased displacement gradients on fault surfaces, as they approach through-going fractures. Together, these relationships suggest that the faults and vertically continuous fractures formed during the same geological event, after deposition of the Middle Jurassic Dogger and Saltwick formations.

## Jet Rock and Bituminous Shale (Whitby Mudstone Formation) at Saltwick Nab

The Bituminous shale and uppermost Jet rock are exposed in cliffs and platforms at Saltwick Nab (Fig. 2a). The Whitby Mudstone Formation at Saltwick Nab is not cut by faults, and is situated ca. 1500 m to the east of the west-dipping Whitby Harbour fault (i.e. within the footwall).

The Bituminous shale is cut by sub-vertical NNW-SSE and WNW-ESE striking fractures and (rare) shear fractures (Figs 8a, b). Some fractures contain thin calcite fills. Plumose markings and elliptical arrest lines are preserved on the surfaces of NNW-SSE and WNW-ESE fractures (Fig. 8c), which suggests that both sets originated as opening mode fractures. In contrast to Jet Wyke and Port Mulgrave, we have not observed bed-parallel fractures or veins at Saltwick Nab (Fig. 8b). NNW-SSE striking fractures abut WNW-ESE striking structures, and vice versa (Fig. 8d). In places, the two sets of fractures display crossing (“X”) intersections (Fig. 8d), indicating that one of the fractures was closed at the time the other propagated. Quantitative analysis of abutting and cross-cutting relationships suggests that the WNW-ESE fractures more commonly abut NNW-SSE fractures than the opposite relationship (Daniels et al., pers. comm., May 2014). Together, these observations suggest that the NNW-SSE striking fractures developed first, presumably within a stress field characterised by ENE-WSW minimum horizontal stress. Subsequent development of the WNW-ESE striking fractures may have taken place due to anticlockwise rotation of the minimum horizontal stress direction, giving rise to minor shear reactivation and renewed opening-mode propagation of the NNW-SSE fracture set. The timing of fracture development at Saltwick Nab is not well constrained. However, the similarity in inferred extension directions suggests that the NNW-SSE fractures at Saltwick Nab may have initiated at the same time as slip along the NNW-SSE striking faults and fractures at Whitby East Cliff, i.e. following deposition of the Middle Jurassic Dogger and Saltwick formations.

## Analysis

Observations of faults and fractures in the Cleveland Ironstone and Whitby Mudstone formations show that: (1) Sub-vertical fractures and veins occur throughout the Cleveland Basin at Jet Wyke, Port Mulgrave, Whitby East Cliff and Saltwick Nab. (2) Bed-parallel fractures and veins occur preferentially within clay-rich lithologies at Jet Wyke and Port Mulgrave. These bed-parallel structures appear to have developed synchronously with normal faulting. The timing of normal faulting at the studied localities is not constrained precisely, but probably post-dates deposition of the Cleveland Ironstone and Whitby Mudstone formations and, at Whitby East Cliff, deposition of the Middle Jurassic Dogger and Saltwick formations. (3) Bed-parallel fractures are not observed within the Bituminous shale at Saltwick Nab, despite the well-developed bedding planes and clay-rich lithology.

A key problem, therefore, concerns the development of sub-horizontal, bed-parallel fractures at a time when the regional stress field was likely characterised by  $S_v = \sigma_1$  (Lash and Engelder, 2005). The absence of bed-parallel fractures at Saltwick Nab suggests that the presence of well-developed bedding planes – which might suggest a marked, layer-perpendicular strength anisotropy – was not the primary control on bed-parallel fracturing. To address this problem, we start by evaluating the possible causes of fluid overpressure during burial of the Cleveland Ironstone and Whitby Mudstone formations. Next, we consider the relationship between clay content and bed-parallel fracturing, following previous work by Lash and Engelder (2005). We then investigate the possible impact of pre-lithification exhumation of the Whitby Mudstone Formation on the local, latest Toarcian to earliest Aalenian stress field at Saltwick Nab. We conclude that clay content of the host rock and perturbation of the stress field due to normal faulting may have been the main factors that controlled the development and distribution of bed-parallel fractures in the Cleveland Basin.

## Overpressure generation within the Cleveland Basin

Bed-parallel fracturing in horizontally-bedded rocks requires that  $P_p > S_v$ . Loading during burial can generate overpressure due to disequilibrium compaction, particularly during the rapid subsidence of low permeability, e.g. clay-rich sediments (Osborne and Swarbrick, 1997). However, the slow burial rate during the Early Jurassic and subsequently suggests that disequilibrium compaction is unlikely to have been the primary cause of overpressure within the Cleveland Basin.

Conversion of kerogen to hydrocarbon was a possible source of overpressure in the Cleveland Basin, consistent with burial of the Whitby Mudstone Formation into the early oil window (French et al., 2014). Sælen et al. (2000) noted the presence of oil in the chambers of ammonites preserved in the Jet rock. We have observed minor oil seeps from vugs along sub-vertical, calcite-filled fractures, and hydrocarbon staining within calcite-filled dilatational jogs along normal faults that cut the Jet rock at Port Mulgrave. Given the maturity of the Whitby Mudstone Formation, any overpressure due to hydrocarbon maturation is likely to have been generated at or close to the maximum burial depth, a scenario consistent with overpressure generation under conditions of (approximately) constant vertical stress.

Kemp et al. (2005) demonstrated that the Whitby Mudstone Formation contains illite-smectite (I-S) mixed layer clays comprising 90 % illite. They suggested detrital smectite was transformed to I-S during burial. We infer that detrital smectite is likely to have been most abundant in clay-rich lithologies (i.e. clay-rich mudstone lithofacies of the Cleveland Ironstone Formation, lowermost Jet rock and the Bituminous shale). Release of structurally-bound water and/or dissolution of load-bearing grains due to conversion of smectite to illite could have contributed to overpressure generation during diagenesis (Osborne and Swarbrick, 1997; Lahann and Swarbrick, 2011). Depending on its

composition, discrete smectite is likely to have disappeared at temperatures  $> 70\text{ }^{\circ}\text{C}$  (Boles and Franks, 1979), which suggests that any contribution to overpressure caused by smectite to illite conversion may have initiated prior to or synchronous with oil generation in the Cleveland Basin.

### Bed-parallel fracturing in clay-rich units

Lash and Engelder (2005) presented a detailed study of bed-parallel microfractures within the Upper Devonian Dunkirk Shale Member, New York State. They hypothesised that the local stress state within clay-rich layers may have favoured propagation of horizontal microfractures during burial, i.e. locally  $S_h > S_v$ . According to Lash and Engelder (2005), propagation of either horizontal or vertical opening mode fractures depends on the local uniaxial stress ratio,  $R$  ( $R = S_h / S_v$ ), at the time of cementation, and the subsequent stress path,  $\kappa$  ( $\kappa = \Delta S_h / \Delta P_p$ ), followed by the rock in  $S_h$  versus  $P_p$  space after cementation (Table 1). Propagation of vertical fractures is favoured when the stress path intersects the  $S_h = P_p$  line and  $R < 1$  (i.e.  $S_h < S_v$ ). Propagation of horizontal fractures is favoured when the stress path intersects the  $\lambda = 1$  line ( $\lambda = P_p / S_v$ ) and  $R > 1$  (i.e.  $S_h > S_v$ ) (Fig. 9). In general, drained compaction of clay-rich sediment will yield higher  $R$  values compared to drained compaction of sandy sediment (Lash and Engelder, 2005). In all cases, disequilibrium compaction will yield higher stress ratios than drained compaction (Fig. 9). Thus, depending on the slope of the stress path,  $\kappa$ , horizontal fractures are more likely to propagate within overpressured clay-rich lithologies subjected to disequilibrium compaction, than in sand-rich lithologies subjected to drained compaction (Lash and Engelder, 2005; Fig. 9).

Lash and Engelder (2005) assumed that: (1) vertical stress was constant during pore pressure build-up within lithified Dunkirk Shale Member; (2) Dunkirk Shale Member underwent drained or undrained compaction prior to cementation; and (3)  $S_h$  and  $P_p$  were

coupled after lithification, due to poroelastic deformation. Under these circumstances,  $P_p$ -driven changes in  $S_h$  follow a stress path,  $\kappa$ , given by:

$$\kappa = \frac{\Delta S_h}{\Delta P_p} = \alpha \frac{1-2\nu}{1-\nu} \quad (\text{Lash and Engelder, 2005}) \quad (1)$$

where  $\alpha$  is the Biot coefficient and  $\nu$  is Poisson's ratio. We now consider the extent to which these assumptions were met during burial within the Cleveland Basin.

Overpressure is likely to have developed when the Cleveland Ironstone and Whitby Mudstone formations approached their maximum burial depths. Of course, we cannot rule out a contribution to overpressure due to diagenesis and/or maturation of the underlying, more deeply buried Redcar Mudstone Formation (Sinemurian to Pliensbachian) (TOC 0.4% to 1.4%; van Buchem et al., 1995). Nevertheless, the low burial rate within the Cleveland Basin suggests that the assumption of (approximately) constant  $S_v$  during fracturing is not unreasonable.

Normal compaction occurs when horizontally-bedded sediment undergoes purely vertical reduction in thickness. The horizontal stresses are isotropic during normal compaction, and the ratio of horizontal effective stress to vertical effective stress is known as the coefficient of earth pressure at rest, ( $K_o$ ), defined as:

$$K_o = \frac{S_h - P_p}{S_v - P_p} \quad (\text{e.g. Mayne and Kulhawy, 1982; Gouly, 2003}). \quad (2)$$

Normal faulting at Jet Wyke and Port Mulgrave initiated after deposition of the Cleveland Ironstone and Whitby Mudstone formations. At Whitby East Cliff, faulting post-dates deposition of the Middle Jurassic Dogger and Saltwick formations. Normal compaction of sediment could therefore have occurred at these localities during burial during Pliensbachian to Toarcian times, prior to faulting.

According to Jones (1994),  $K_o$  depends on lithology, with typical values  $K_o > 0.7$  for clays,  $0.3 \leq K_o \leq 0.4$  for sands, and intermediate values for silts. The stress ratio,  $R$ , for

consolidated sediment can be calculated from  $K_0$ :

$$R = \frac{S_h}{S_v} = \frac{K_0(S_v - P_p) + P_p}{S_v} \quad (\text{Lash and Engelder, 2005}). \quad (3)$$

During normal compaction this variability in  $K_0$  means that clay-rich sediment – such as the Bituminous shale and clay-rich mudstone units of the Cleveland Ironstone Formation (see Fig. 3) – are characterised by a higher horizontal to vertical stress ratio ( $R$ ) than sediment with lower clay content – such as the Cement shale and sand-rich mudstone and concretionary carbonate units of the Cleveland Ironstone Formation (Fig. 3) – assuming the same pore pressure gradient.

Finally, we consider the likelihood that  $P_p$  and  $S_h$  were coupled due to poroelastic deformation following cementation of the Cleveland Ironstone and Whitby Mudstone formations. Poroelastic deformation assumes uniaxial strain, an assumption that may be valid for Saltwick Nab, which has not been affected by faulting. However, the Cleveland Ironstone and Whitby Mudstone formations at Jet Wyke, Port Mulgrave and Whitby East Cliff carry the effects of normal faulting. Here,  $S_h$  may have been controlled by the coefficient of sliding friction on adjacent faults rather than by poroelastic deformation during purely passive subsidence. Assuming plane strain conditions and that the faults were critically-stressed, cohesionless and optimally oriented for slip according to the Coulomb failure criterion,  $S_h$  is given by:

$$S_h = S_v \left( \frac{1 - \sin\phi}{1 + \sin\phi} \right) + 2P_p \left( \frac{\sin\phi}{1 + \sin\phi} \right), \quad (4a)$$

for  $\nu > \frac{1 - \sin\phi}{2}$ , in which case  $S_h$  acts parallel to the dip direction of the fault; or

$$S_h = \left( \frac{1}{1 + \sin\phi} \right) \left( 2\nu S_v - P_p(2\nu - 1 - \sin\phi) \right), \quad (4b)$$

for  $\nu < \frac{1 - \sin\phi}{2}$ , in which case  $S_h$  acts parallel to fault strike, where  $\phi$  is the friction angle and other parameters are as given above (Addis et al., 1996).

Under these circumstances,  $P_p$ -driven changes in  $S_h$  follow a stress path,  $\kappa_f$ , given by:

$$\kappa_f = \frac{\Delta S_h}{\Delta P_p} = 2 \frac{\sin\phi}{1+\sin\phi}, \quad (5a)$$

for  $\nu > \frac{1-\sin\phi}{2}$ , or

$$\kappa_f = \frac{\Delta S_h}{\Delta P_p} = \frac{\sin\phi+1-2\nu}{1+\sin\phi} \quad (5b)$$

for  $\nu < \frac{1-\sin\phi}{2}$ , and assuming constant  $S_v$ .

Figure 10 shows the hypothetical stress paths,  $\kappa_f$ , for plausible friction angles and Poisson's ratios. Shallower stress paths, which favour propagation of vertical fractures, result from moderate to high Poisson's ratio and low friction angles. In this case, higher Poisson's ratios cause  $S_h$  to act parallel to the dip direction of the fault, a necessary condition for propagation of vertical fractures whose strike is parallel to that of the controlling fault. Steeper stress paths, which favour propagation of horizontal (bed-parallel) fractures may result from a range of friction angles and Poisson's ratios. These results support the hypothesis that changes in  $S_h$  driven by changes in  $P_p$  within normally-faulted basins can lead to propagation of horizontal fractures in overpressured, clay-rich sedimentary rocks (Fig. 10b). We postulate that such conditions existed within clay-rich mudstone units of the Cleveland Ironstone Formation at Jet Wyke and the Bituminous shale at Port Mulgrave.

The sub-vertical fractures within the Cement shale at Whitby East Cliff probably developed as a result of the lower clay content within this unit. Additionally, the Cement shale lies directly below the uppermost Toarcian to lowermost Aalenian unconformity, and is juxtaposed against the sandy, more permeable Middle Jurassic Saltwick Formation in the hanging wall of the adjacent Whitby Harbour fault (Alexander and Gawthorpe, 1993). The Cement shale could therefore have been drained, resulting in reduced  $P_p$ . The proximity to the Whitby Harbour fault may also have resulted in elevated differential stress at this

locality, giving rise to the network of small-scale normal faults.

### Exhumation and reburial at Saltwick Nab

The foregoing analysis can explain the occurrence of bed-parallel fractures at Jet Wyke and Port Mulgrave, but does not explain why these structures are absent from the – presumably – clay-rich Bituminous shale at Saltwick Nab. It is possible that lateral facies variations gave rise to lower clay content within the Bituminous shale at Saltwick Nab, but this hypothesis remains untested. The sediments at Saltwick Nab (and Whitby East Cliff) did, however, experience up to 60 m exhumation during latest Toarcian to earliest Aalenian times, prior to lithification and cementation (Powell, 2010). During exhumation and subsequent re-burial, laboratory data (Mayne and Kulhawy, 1982) indicate that  $K_o$  is a function of friction angle ( $\phi$ ) and the over-consolidation ratio (OCR), where:

$$OCR = \frac{(S_v - P_p)_{\text{maximum}}}{(S_v - P_p)_{\text{minimum}}} \quad (6)$$

We have used an empirical relationship between  $K_o$  and OCR (equation 18 of Mayne and Kulhawy, 1982) to estimate the change in stress ratio,  $R$ , caused by latest Toarcian to earliest Aalenian exhumation and re-burial of the then-unlithified sediments at Whitby East Cliff and Saltwick Nab (Fig. 11). Assuming: (1) a friction angle of  $23^\circ$  (which yields a stress ratio  $R = 0.79$  during initial burial, taken from the stress ratio for silty clay in the Dunkirk Shale Member; Lash and Engelder, 2005); (2) exhumation of 60 m (Powell, 2010); and (3) hydrostatic pore pressure as well as lithostatic and hydrostatic gradients cited by Lash and Engelder (2005), then  $R > 1$  for exhumation to within  $< 15$  m of the surface. During re-burial,  $R$  decreases rapidly within the first 10 m of burial before approaching a near-constant value, in this case slightly below the stress ratio for initial burial (Fig. 11). These relationships suggest that the stress ratio ( $R$ ) at Saltwick Nab (and Whitby East Cliff) could have exceeded the stress ratios at Jet Wyke and Port Mulgrave (Fig. 9), assuming

cementation occurred within 10 m of the surface during reburial. Such elevated stress ratios would have increased the likelihood of horizontal fracture propagation within the clay-rich Bituminous shale, which is inconsistent with our observations from Saltwick Nab. It is more likely that the lack of bed-parallel fractures at Saltwick Nab means that pore fluid pressures in these deposits never exceeded  $S_v$  (Fig. 9), perhaps as a consequence of the relatively deep exhumation of this region and the ensuing stratigraphic proximity of the Bituminous shale to the overlying, more permeable (Alexander and Gawthorpe, 1993) and potentially drained sandstones of the Middle Jurassic Saltwick Formation.

### **Normal faulting at Jet Wyke and Port Mulgrave**

The association between bed-parallel fractures and normal faults at Jet Wyke and Port Mulgrave, and the lack of both types of structure at Saltwick Nab, suggests there may be a causal relationship between normal faulting and bed-parallel fracturing. We test this hypothesis using an elastic dislocation model to estimate the stresses and predicted orientation and distribution of tensile fractures in the foot- and hanging walls of an idealised, normal fault embedded in an isotropic, elastic half space (Healy et al., 2004; Dee et al., 2007; Fig. 12).

In elastic dislocation theory, faults are modelled as surfaces across which there is a discontinuity in the elastic displacement field. The surrounding volume is assumed to have zero displacement at an infinite distance from the fault. In our model, the maximum fault slip is assumed to be  $< 5$  m on a planar, elliptical fault surface with a length of ca. 2 km. The point of maximum slip lies at the centre of the fault plane and slip decreases elliptically towards the fault tip line (Fig. 12). This configuration yields a slip to length ratio of ca.  $10^{-3}$ , which is at the upper limit of elastic deformation within the Earth's crust. The fault dips at  $69^\circ$  and the shallowest point on its tip line is buried 500 m below the free surface. Poisson's ratio of the elastic medium is 0.32. The model predicts tensile fractures will

occur within the upper part of the fault hanging wall above the point of maximum slip, presumably as a result of dilatational strains necessary to accommodate the displacement gradient on the fault surface (see fig. 1c of Barnett et al., 1987). This zone of fracturing extends outwards from the fault plane into the hanging wall to a distance of ca. 10% of the fault length. Tensile fractures adjacent to the fault tip line dip at ca. 45° in a direction approximately parallel to fault strike. Towards the centre of the fault, the dip of fractures decreases (to ca. 3°) and the dip direction of the fractures becomes parallel to the fault dip direction (Fig. 12). A less-well developed zone of gently-dipping tensile fractures is also predicted in the lower part of the footwall (i.e. behind the fault plane shown in Fig. 12).

These gently-dipping tensile fractures in the foot- and hanging walls of the modelled fault plane are reminiscent of the bed-parallel fractures we observed at Jet Wyke and Port Mulgrave. We propose that the propensity for bed-parallel fracturing within clay-rich units at these localities – characterised by elevated  $P_p$  and  $S_h > S_v$  – was further enhanced by the local stress perturbations within the upper parts of the hanging walls, or lower parts of the footwalls, of adjacent normal faults.

## Discussion

Our results are consistent with the hypothesis that horizontal fractures are more likely to develop in clay-rich sedimentary rocks (Lash and Engelder, 2005). This conclusion depends upon the maintenance of fluid overpressure within clay-rich units, and the proximity to an active fault. A pertinent question is why did the presence of open, bed-parallel fractures not drain  $P_p$ ? One possibility is that the bed-parallel fractures were only partially open at any given moment. It is also possible that these fractures are limited in their areal extent. If, as seems to be the case, individual bed-parallel fractures are limited to fault-bounded blocks, lateral drainage may have been prevented if the faults acted as

seals. Contrary to this suggestion is our observation of vuggy calcite- and bitumen-filled veins along fault slip surfaces, which implies that at times, faults acted as conduits for fluid flow. However, the length scale of fluid transport within faults is unclear.

Another outstanding problem relates to the apparently regular spacing of bed-parallel fractures in the Bituminous shale. Overall, the Bituminous shale is clay-rich (Fig. 3) – but what controls the distribution of bed-parallel fractures within this unit? Detailed lithofacies descriptions for the thinly-bedded Bituminous shale are not yet available. However, the similarity between spacings of bed-parallel fractures and the 60 cm and 112 cm wavelengths in cyclicity in  $\text{CaCO}_3$  and TOC (Kemp et al., 2011) lead us to speculate that subtle, cyclic variations in mineralogy – and, more specifically, clay content – may control the fracture distribution.

More generally, our results highlight the likely structural complexity of prospective UK shale basins and concur with many previous studies that emphasise the need to integrate structural, stratigraphic, diagenetic and burial histories for successful fracture characterisation (e.g. Laubach et al., 2010). Even ignoring the inversion-related structures, the Cleveland Basin displays a range of fractures whose prediction depends on a detailed knowledge of the burial, exhumation, cementation and faulting histories across the basin, in addition to variations in clay content within mudstone-dominated sequences.

Paradoxically, some of the structural complexity may have arisen because the Cleveland Basin was characterized by gentle subsidence and slow burial rates throughout much of the Early and Middle Jurassic. As a result, localised uplift events resulted in erosion and exhumation of the Whitby Mudstone Formation, leading to variations in fluid pressure gradients and overpressure development.

Finally, it is worth emphasising that the Whitby Mudstone Formation is marginally mature for oil, but the prospective Bowland-Hodder shale unit in northern England is mature for gas. Gas cracking (e.g. Osborne and Swarbrick, 1997) may have resulted in greater

overpressures within the Bowland-Hodder shale unit compared to the Whitby Mudstone Formation, leading to more widespread development of bed-parallel fractures within the former unit. However, there is unlikely to be a direct correspondence between structures observed within the Cleveland Ironstone and Whitby Mudstone formations and the Bowland-Hodder shale unit. For example, the Bowland Shale Formation in NE England underlies a sequence of Permian evaporites that, at least in part, detaches the Jurassic cover from the Carboniferous “basement”. Furthermore, the Carboniferous is cut by mainly E-W, rather than NNW-SSE striking faults, which suggests that the structural response to Jurassic extension and latest Cretaceous to Neogene inversion may have been very different in the Carboniferous and Jurassic successions. Nevertheless, our study highlights the likely sensitivity of natural fracture development within the Bowland-Hodder shale unit to variations in fluid pressure gradients and local stress ratios.

## Conclusions

1. The Cleveland Basin overlies a Mississippian depocentre that locally contains > 3000 m of Bowland-Hodder shale unit in NE England. As such, faults and fractures within the Lower Jurassic Cleveland Ironstone (Pliensbachian) and Whitby Mudstone (Toarcian) formations may provide insights into the post-Triassic tectonic history of the poorly-exposed Bowland-Hodder shale unit. We present field observations of faults and fractures within the Cleveland Ironstone and Whitby Mudstone formations at four, well-exposed coastal localities in North Yorkshire: Jet Wyke, Port Mulgrave, Whitby East Cliff and Saltwick Nab.
2. The Cleveland Ironstone and Whitby Mudstone formations were deposited in the Cleveland Basin. Average burial rates were low ( $< 20 \text{ m Myr}^{-1}$ ) throughout the Early Jurassic, and tectonic subsidence was mainly a response to thermal re-equilibration of the

lithosphere following latest Permian to earliest Triassic rifting. Previous authors have recognised syn-sedimentary normal faults throughout the Cleveland Basin (Runswick Bay, Whitby Harbour and Peak faults), which were active during the Early, Middle and Late Jurassic. However, minor normal faults at Jet Wyke, Port Mulgrave and Whitby East Cliff all initiated after the Cleveland Ironstone and Whitby Mudstone Formation sediments were deposited. Normal faults have not been observed at Saltwick Nab.

3. Sets of opening-mode bed-parallel fractures, some of which contain blocky calcite fills, cut clay-rich units within the Cleveland Ironstone and Whitby Mudstone formations at Jet Wyke and Port Mulgrave, respectively. Cutting and branching relationships suggest that the bed-parallel fractures developed synchronously with normal faulting at these localities, i.e. within a regional stress field in which  $S_v = \sigma_1$ . Propagation of bed-parallel fractures requires that  $P_p > S_v$  and a local stress field within clay-rich units in which  $S_h > S_v$ . Bed-parallel fractures have not been observed within bioturbated, clay-poor Cement shale (Whitby Mudstone Formation) at Whitby East Cliff, or within well-bedded, clay-rich Bituminous shale (Whitby Mudstone Formation) at Saltwick Nab.

4. Sets of sub-vertical fractures, some of which contain thin calcite fills, occur within the Cleveland Ironstone Formation at Jet Wyke and within the Whitby Mudstone Formation at Port Mulgrave, Whitby East Cliff and Saltwick Nab. The surfaces of these fractures carry plumose markings and concentric arrest lines, consistent with an opening mode origin. At Jet Wyke and Port Mulgrave, the sub-vertical fractures display curving-parallel and curving-perpendicular relationships with the bed-parallel fractures, which suggests that the bed-parallel fractures were, at times, open and acting as free surfaces. At Whitby East Cliff, the sub-vertical fractures cross-cut the overlying, uppermost Toarcian to lowermost Aalenian unconformity, and also link with minor normal faults (cm-scale displacements) within the Cement shale (Whitby Mudstone Formation) in the footwall of the adjacent, syn-sedimentary Whitby Harbour fault. At Saltwick Nab, two sets of sub-vertical fractures

display an apparently conjugate pattern in map view. However, analysis of crossing and abutting relationships suggests that the NNW-SSE striking fractures formed first, followed by WNW-ESE striking fractures that probably developed in response to an anticlockwise rotation of  $S_h$ . In all cases, propagation of sub-vertical fractures requires that  $P_p = S_h$ .

5. According to Lash and Engelder (2005), normal compaction can lead to higher uniaxial stress ratios ( $S_h / S_v$ ) in clay-rich sediment compared to sand-rich sediment. Following cementation, coupling between  $P_p$  and  $S_h$  may have been driven by poroelastic deformation or incipient slip along critically stressed normal faults, causing local elevation of the in situ horizontal stress in excess of the vertical stress, allowing bed-parallel fractures to propagate within clay-rich units within the Cleveland Ironstone and Whitby Mudstone formations at Jet Wyke and Port Mulgrave. Dilatational strains adjacent to normal faults may have further enhanced the likelihood of bed-parallel fracturing within faulted, clay-rich units.

6. The local absence of normal faulting may, in part, explain the lack of bed-parallel fractures at Saltwick Nab, despite the well-developed bedding plane anisotropy. In addition, partial exhumation of the Whitby Mudstone Formation along the uppermost Toarcian to lowermost Aalenian unconformity led to deposition of permeable, potentially drained Middle Jurassic Saltwick Formation sandstones immediately above the Whitby Mudstone Formation at Saltwick Nab and Whitby East Cliff. The bioturbated Cement shale (Whitby Mudstone Formation) at Whitby East Cliff is also juxtaposed against Saltwick Formation sandstones in the hanging wall of the adjacent Whitby Harbour fault. The structural and stratigraphical proximity of Saltwick Formation sandstone at Saltwick Nab and Whitby East Cliff may have drained the Whitby Mudstone Formation, preventing the development of large fluid overpressures ( $P_p = S_v$ ) required for bed-parallel fracturing.

7. Our findings suggest that fracture patterns in UK shale basins are likely to be heterogeneous over distances  $< 15$  km, which is on a scale smaller than some existing UK

Petroleum Exploration and Development Licenses within Bowland-Hodder shale unit resource area. This heterogeneity arises from stratigraphical variations in mineralogy (e.g. clay content), bedding plane anisotropy, the distribution of faults and differential exhumation across the basin. We emphasise the necessity that fracture characterization studies integrate structural geology with analyses of the stratigraphic, diagenetic and burial histories of prospective sedimentary basins.

## References Cited

Addis, M.A., Last, N.C., and Yassir, N.A., 1996, Estimation of Horizontal Stresses at Depth in Faulted Regions and Their Relationship to Pore Pressure Variations: *Journal of Formation Evaluation*, v. 48, p. 11-18.

Alexander, J., 1986, Idealised flow models to predict alluvial sandstone body distribution in the Middle Jurassic Yorkshire Basin: *Marine and Petroleum Geology*, v. 3, p. 298-305.

Alexander, J., and Gawthorpe, R.L., 1993, The complex nature of a Jurassic multistorey, alluvial sandstone body, Whitby, North Yorkshire, in C.P. North and D.J. Prosser, *Characterization of Fluvial and Aeolian Reservoirs*, Special Publication no. 73: London, UK, Geological Society, p. 123-142.

Anderson, E.M., 1951, *The Dynamics of Faulting and Dyke Formation with Applications to Britain*: Edinburgh, UK, Oliver and Boyd, 206 p.

Andrews, I.J., 2013, *The Carboniferous Bowland Shale gas study: geology and resource estimation*: London, UK, British Geological Survey for Department of Energy and Climate Change, 64 p.

Aoudia, K., Miskimins, J.L., Harris, N.B., and Mnich, C.A., 2010, *Statistical Analysis of the Effects of Mineralogy on Rock Mechanical Properties of the Woodford Shale and the*

Associated Impacts for Hydraulic Fracture Treatment Design, Conference Paper 10-303, 44th US Rock Mechanics Symposium and 5th US-Canada Rock Mechanics Symposium, Salt Lake City, UT, American Rock Mechanics Association, 11 p.

Bahat, D., and Engelder, T., 1984, Surface morphology on cross-fold joints of the Appalachian Plateau, New York and Pennsylvania: *Tectonophysics*, v. 104, p. 299-313.

Boles, J.R, and Franks, S.G., 1979, Clay diagenesis in Wilcox sandstones of southwest Texas: implications of smectite diagenesis on sandstone cementation: *Journal of Sedimentary Petrology*, v. 49, p. 55-70.

Barnett, J.A.M., Mortimer, J., Rippon, J.H., Walsh, J.J., and Watterson, J., 1987, Displacement Geometry in the Volume Containing a Single Normal Fault: *AAPG Bulletin*, v. 71, p. 925-937.

Bons, P.D., Elburg, M.A., and Gomez-Rivas, E., 2012, A review of the formation of tectonic veins and their microstructures: *Journal of Structural Geology*, v. 43, p. 33-62.

Bray, R.J., Green, P.F., and Duddy, I.R., 1992, Thermal history reconstruction using apatite fission track analysis and vitrinite reflectance: a case study from the UK East Midland and Southern North Sea, in R.F.P. Hardman, *Exploration Britain: Geological insights for the next decade*, Special Publication no. 67: London, UK, Geological Society, p. 3-25.

Chadwick, R.A., and Evans, D.J., 1995, The timing and direction of Permo-Triassic extension in southern Britain, in S.A.R. Boldy, ed., *Permian and Triassic rifting in Northwest Europe*, Special Publication no. 91: London, UK, Geological Society, p. 161-192.

Chadwick, R.A., and Holliday, D.W., 1991, Deep crustal structure and Carboniferous basin development within the Iapetus convergence zone, northern England: *Journal of the Geological Society*, v. 148, p. 41–53.

Cox, B.M., Sumblar, M.G., and Ivimey-Cook, H.C., 1999, A formational framework for the

Lower Jurassic of England and Wales (onshore area): Keyworth, Notts., UK, British Geological Survey Research Report, RR/99/01, 30 p.

Dee, S.J., Yielding, G., Freeman, B., Healy, D., Kusznir, N.J., Grant, N., and Ellis, P., 2007, Elastic dislocation modelling for prediction of small-scale fault and fracture network characteristics *in* L. Lonergan, Jolly, R.J.H, Rawnsley, K., and D.J. Sanderson, eds., Fractured Reservoirs, Special Publication no. 270: London, UK, Geological Society, p. 139-155.

Department of Trade and Industry, 2003, The hydrocarbon prospectivity of Britain's onshore basins: London, UK, British Geological Survey for Department of Trade and Industry, 93 p.

Department of Energy and Climate Change, 2014, Exploration and production - Oil and gas: onshore maps and GIS shapefiles, < <https://www.gov.uk/oil-and-gas-onshore-maps-and-gis-shapefiles>> Accessed April 14, 2014.

Dixon, A.D.G., 1989, Evolution of the Yorkshire, Sole Pit and East Midland basin systems, UK, PhD thesis, Durham University, Durham, UK, 210 p.

Dyer, R., 1988, Using joint interactions to estimate paleostress ratios: *Journal of Structural Geology*, v. 10, p. 685-699.

Engelder, T., 1993, *Stress Regimes in the Lithosphere*: Princeton, NJ, Princeton University Press, 492 p.

Engelder, T., Lash, G.G., Uzcátegui, R.S., 2009, Joint sets that enhance production from Middle and Upper Devonian gas shales of the Appalachian Basin: *AAPG Bulletin*, v. 93, p. 857-889.

Fraser, A.J., and Gawthorpe, R.L., 2003, *An Atlas of Carboniferous Basin Evolution in Northern England*: memoir no. 28, London, UK, Geological Society, 79 p.

French, K.L., Sepúlveda, J., Trabucho-Alexandre, J., Gröcke, D.R., and Summons, R.E., Organic geochemistry of the early Toarcian oceanic anoxic event in Hawsker Bottoms, Yorkshire, England: *Earth and Planetary Science Letters*, v. 390, p. 116-127.

Gad, M.A., Catt, J.A., and Le Riche, H.H., 1968, Geochemistry of the Whitbian (Upper Lias) sediments of the Yorkshire Coast: *Proceedings of the Yorkshire Geological Society*, v. 37, p. 105-140.

Gale, J.F.W., Reed, R.M., and Holder, J., 2007, Natural fractures in the Barnett Shale and their importance for hydraulic fracture treatments: *AAPG Bulletin*, v. 91, p. 603-622.

Goult, N.R., 2003, Reservoir stress path during depletion of Norwegian chalk oilfields: *Petroleum Geoscience*, v. 9, p. 233-241.

Green, P.F., 1989, Thermal and tectonic history of the East Midlands shelf (onshore UK) and surrounding regions assessed by apatite fission track analysis: *Journal of the Geological Society*, v. 146, p. 755-773.

Healy, D., Yielding, G., and Kuszniir, N., 2004, Fracture prediction for the 1980 El Asnam, Algeria earthquake via elastic dislocation modeling: *Tectonics*, v. 23, TC6005, doi:10.1029/2003TC001575, 21 p.

Hemingway, J.E., and Riddler, G.P., 1982, Basin inversion in north Yorkshire: *Transactions of the Institute of Mining and Metallurgy, Section B*, v. 91, p. 175–186.

Holliday, D.W., 1999, Palaeotemperatures, thermal modelling and depth of burial studies in northern and eastern England: *Proceedings of the Yorkshire Geological Society*, v. 52, p. 337-352.

Howarth, M.K., 1955, Domes of the Yorkshire Coast: *Proceedings of the Yorkshire Geological Society*, v. 30, p. 147-175.

Howarth, M.K., 1962, The Jet Rock and the Alum Shale Series of the Yorkshire Coast:

Proceedings of the Yorkshire Geological Society, v. 33, p. 381-422.

Jeans, C.V., 2006, Clay mineralogy of the Jurassic strata of the British Isles: *Clay Minerals*, v. 41, p. 187-307.

Jones, M.E., 1994. Mechanical principles of sediment deformation, in A.Maltman, *The Geological Deformation of Sediments*: London, UK, Chapman and Hall, p. 37–71.

Kemp, D.B., Coe, A.L., Cohen, A.S., and Schwark, L., 2005, Astronomical pacing of methane release in the Early Jurassic period: *Nature*, v. 427, p. 396-399.

Kemp, D.B., Coe, A.L., Cohen, A.S., and Weedon, G.P., 2011, Astronomical forcing and chronology of the early Toarcian (Early Jurassic) oceanic anoxic event in Yorkshire, UK: *Palaeogeography, v. 26, PA4210, doi:10.1029/2011PA002122.*

Kemp, S.J., Merriman, R.J., and Bouch, J.E., 2005, Clay mineral reaction progress – the maturity and burial history of the Lias Group of England and Wales: *Clay Minerals*, v. 40, p. 43-61.

Lahann, R.W., and Swarbrick, R.E., 2011, Overpressure generation by load transfer following shale framework weakening due to smectite diagenesis: *Geofluids*, v. 11, p. 362-375.

Lash, G.G., and Engelder, T., 2005, An analysis of horizontal microcracking during catagenesis: Example from the Catskill delta complex: *AAPG Bulletin*, v. 89, p. 1433-1449.

Laubach, S.E., Eichhubl, P., Hilgers, C., and Lander, R.H., 2010, Structural diagenesis: *Journal of Structural Geology*, v. 32, p. 1866-1872.

Macquaker, J.H.S., and Taylor, K.G., 1996, A sequence-stratigraphic interpretation of a mudstone-dominated succession: the Lower Jurassic Cleveland Ironstone Formation, UK: *Journal of the Geological Society*, v. 153, p. 759-770.

Mayne, P.W., and Kulhawy, F.H., 1982,  $K_0$ -OCR relationships in soil: *Journal of*

Geotechnical Engineering, v. 108, p. 851-872.

McArthur, J.M., Algeo, T.J., van de Schootbrugge, B., Li, Q, and Howarth, R.J., 2008, Basinal restriction, black shales, Re-Os dating, and the Early Toarcian (Jurassic) oceanic anoxic event: *Paleocenanography*, v. 23, PA4217, doi:10.1029/2008PA001607.

Milsom, J., and Rawson, P.F., 1989, The Peak Trough – a major control on the geology of the North Yorkshire coast: *Geological Magazine*, v. 126, p. 699–705.

Osborne, M.J., and Swarbrick, R.E., 1997, Mechanisms for generating overpressure in sedimentary basins: a reevaluation: *AAPG Bulletin*, v. 81, p. 1023-1041.

Pashin, J.C., Kopaska-Merkel, D.C., Arnold, A.C., McIntyre, M.R., and Thomas, W.A., 2012, Gigantic, gaseous mudwads in Cambrian shale: Conasauga Formation, southern Appalachians, USA: *International Journal of Coal Geology*, v. 103, p. 70-91.

Powell, J.H., 1984, Lithostratigraphical nomenclature of the Lias Group in the Yorkshire Basin: *Proceedings of the Yorkshire Geological Society*, v. 45, p. 51-57.

Powell, J.H., 2010, Jurassic sedimentation in the Cleveland Basin: a review: *Proceedings of the Yorkshire Geological Society*, v. 58, p. 21-72.

Pye, K., and Krinsley, D.H., 1986, Microfabric, mineralogy and early diagenetic history of the Whitby Mudstone Formation (Toarcian), Cleveland Basin, UK: *Geological Magazine*, v. 123, p. 191-203.

Raiswell, R., 1976, The microbiological formation of carbonate concretions in the Upper Lias of NE England: *Chemical Geology*, v. 18, p. 227-244.

Raiswell, R., 1982, Pyrite texture, isotopic composition and the availability of iron: *American Journal of Science*, v. 282, p. 1244-1263.

Raiswell, R., and White, N.J.M., 1978, Spatial aspects of concretionary growth in the Upper Lias of northeast England: *Sedimentary Geology*, v. 20, p. 291-300.

Ratcliffe, K., Wright, M., and Spain, D., 2012, Unconventional Methods For Unconventional Plays: Using Elemental Data To Understand Shale Resource Plays, Part 2: PESA News Resources, p. 55-60.

Rawnsley, K.D., Rives, T., Petit, J.-P., Hencher, S.R., and Lumsden, A.C., 1992, Joint development in perturbed stress fields near faults: *Journal of Structural Geology*, v. 14, p. 939-951.

Rawson, P.F., and Wright, J.K., 1996, Jurassic of the Cleveland Basin, North Yorkshire, in P.D. Taylor, *Field Geology of the British Jurassic*: London, UK, Geological Society, p. 173-208.

Rawson, P.F., and Wright, J.K., 2000, *The Yorkshire Coast, Geologists' Association Guide No. 34*: London, UK, The Geologists' Association, 130 p.

Rickman, R., Mullen, M., Petre, E., Grieser, B., and Kundert, D., 2008, A Practical Use of Shale Petrophysics for Stimulation Design Optimization: All Shale Plays Are Not Clones of the Barnett Shale: Conference Paper 115258, SPE Annual Technical Conference and Exhibition, Denver, CO, Society of Petroleum Engineers, 11 p.

Sælen, G., Tyson, R.V., Telnæs, N., and Talbot, M.R., 2000, Contrasting watermass conditions during deposition of the Whitby Mudstone (Lower Jurassic) and Kimmeridge Clay (Upper Jurassic) formations, UK: *Palaeogeography, Palaeoclimatology, Palaeoecology*, v. 163, p. 163-196.

Taylor, K.G., and Macquaker, J.H.S., 2000, Early diagenetic pyrite morphology in a mudstone-dominated succession: the Lower Jurassic Cleveland Ironstone Formation, eastern England: *Sedimentary Geology*, v. 131, p. 77-86.

Thiercelin, M., and Makkhyu, E., Stress field in the vicinity of a natural fault activated by the propagation of an induced hydraulic fracture: Conference Paper 07-201, 1st Canada-US Rock Mechanics Symposium, Vancouver, Canada, American Rock Mechanics

Association, 9 p.

van Buchem, F.S.P., de Boer, P.L., McCave, I.N., and Herbin, J.-P., 1995, The Organic Carbon Distribution in Mesozoic Marine Sediments and the Influence of Orbital Climatic Cycles (England and Western North Atlantic), *in* Huc, A.-Y., ed., *Paleogeography, Paleoclimate, and Source Rocks: AAPG Studies in Geology* 40, p. 303-335.

Warpinski, N.R., Mayerhofer, M.J., Vincent, M.C., Cipolla, C.L., and Lolon, E.P., 2009, Stimulating Unconventional Reservoirs: Maximizing Network Growth While Optimizing Fracture Conductivity: *Journal of Canadian Petroleum Technology*, v. 48, p. 39-51.

Williams, P.F.V., 1986, Petroleum geochemistry of the Kimmeridge Clay of onshore southern and eastern England: *Marine and Petroleum Geology*, v. 3, p. 258-281.

Ziegler, P.A., 1982, *Geological Atlas of Western and Central Europe*: Maatschappij, Netherlands, Shell International Petroleum, Elsevier.

Zijp, M., ten Veen, J., Ventura, D., Verreussel, R., van Laerhoven, L., and Boxem, T., 2014, New Insights From Jurassic Shale Characterization: Strengthen Subsurface Data With Outcrop Analogues: Society of Petroleum Engineers, 14UNCV-167736-MS, 8 p.

Zoback, M.D., Kohli, A., Das, I., and McClure, M., 2012, The Importance of Slow Slip on Faults During Hydraulic Fracturing Stimulation of Shale Gas Reservoirs: Society of Petroleum Engineers, 155476, 9 p.

## Author biographies

Jonathan Imber is a Senior Lecturer in Structural Geology at Durham University. He currently holds a Royal Society Industry Fellowship, in association with Badley Geoscience Ltd. and Geospatial Research Ltd. He previously worked for the Fault Analysis Group at Liverpool University and University College Dublin, having obtained a PhD in Structural Geology from Durham University in 1998.

Howard Armstrong obtained a first degree in geology from Sheffield University before MSc and doctoral research in Palaeozoic palynology and micropalaeontology. His research focuses on understanding extreme climate events, including the origin of Palaeozoic black shale. He has worked on Palaeozoic basins in Europe, South Africa, North Greenland and North Africa and on industry-funded regional petroleum-related projects.

Sarah Clancy obtained a First Class degree in geology at Durham University. She then joined Durham Energy Institute researching the issue of shale gas and oil exploitation using fracking methods and its potential risks. Sarah currently works between Durham and Kuala Lumpur as a geologist for Ikon GeoPressure producing geologically-driven pressure models for different regions around the world.

Susan Daniels obtained her PhD on strike slip processes and responses at convergent margins from Liverpool University in 1998. She subsequently joined ExxonMobil as an Exploration and Production Geoscientist. Susie has been a Senior Geologist at Geospatial Research Ltd. since 2007, where her current interests involve characterisation of natural fracture parameters and regional tectonic syntheses.

Liam Herringshaw is a postdoctoral research fellow at Durham University, studying the biogenic controls of sedimentological variability in shale systems. His broader research focusses on the ecological and environmental impacts of bioturbation, and the evolution of marine ecosystems. Liam has a BSc (Geology & Physical Geography) from the University of Liverpool and a PhD (Palaeobiology) from the University of Birmingham.

Ken McCaffrey obtained his PhD in structural geology from Durham University in 1990. He completed postdoctoral fellowships at John Hopkins University and Trinity College Dublin before taking up a Lectureship at Kingston University. Ken is currently Professor of Structural Geology and Director of the CeREES Centre for Geoenergy at Durham University.

Joel Rodrigues completed an MSci in Geophysics with Geology at Durham University, graduating in 2013. Since then, Joel has been a Technical Support Analyst for Geological and Geophysical software applications at Halliburton Landmark.

João Trabucho-Alexandre is a sedimentologist. He received his licenciatura in geology from the University of Lisbon in 2003, and his MSc (Sedimentology and Stratigraphy) and PhD (Sedimentology) from Utrecht University in 2007 and 2011, respectively. He has been a NERC-funded postdoctoral research associate at Durham University since 2011. In August 2014, João will return to Utrecht as Assistant Professor in sedimentology.

Cassandra Warren obtained a First Class BSc in Geophysics with Geology from Durham University (2012) and her MSc (with Merit) in Petroleum Geoscience from Imperial College (2013). During her studies, Cassie completed research internships with Durham Energy

Institute, Ikon GeoPressure and Schlumberger. She is currently a Petroleum Systems Geologist with Schlumberger Information Solutions in Aachen.

## Figure Captions

1. Map showing the geographical location of the coastal study areas, roads and settlements, Cleveland Basin, NE England. The traces of syn-sedimentary faults discussed in the text are shown for reference (WHF = Whitby Harbour fault; RBF = Runswick Bay fault). The study areas (arrowed), from north to south, are Jet Wyke, Port Mulgrave, Whitby East Cliff and Saltwick Nab. Locations of the studied outcrops are Jet Wyke [0.7870°W, 54.5580°N to 0.7764°W, 54.5571°N], Port Mulgrave [0.7669°W, 54.5498°N to 0.7639°W, 54.5448°N], Whitby East Cliff [0.5999°W, 54.4903°N to 0.6073°W, 54.4904°N] and Saltwick Nab [0.5921°W, 54.4879°N to 0.5883°W, 54.4866°N]. Map based on a Transverse Mercator projection. The inset shows the location of the coastal section (arrowed box) within Great Britain.
  
2. Diagrams summarising the geological setting of the Cleveland Basin.
  - a. Simplified geological map showing the Jurassic strata and principal structural elements of the Cleveland Basin (modified from Powell, 2010). Faults at outcrop are bold solid lines; faults below the Cretaceous chalk are bold dashed lines. Jurassic syn-sedimentary faults identified by Alexander (1986) are highlighted: Peak fault (PF); Whitby Harbour fault (WHF) and Runswick Bay fault (RBF). Other major structures include Flamborough fault zone (FFZ), Vale of Pickering fault zone (VPFZ), Market Weighton High (MWH), and the axial trace of the Cleveland anticline (CA). Dots – Triassic rocks at outcrop; brickwork – Cretaceous rocks at outcrop; grey – Jurassic at outcrop. The locations of onshore boreholes in (b) are starred: Staithes 4 (S); Robin Hood's Bay 1 (R); Fordon 1 (F).
  
  - b. Backstripped, tectonic subsidence curves for the Staithes 4, Robin Hood's Bay 1 and Fordon 1 boreholes (borehole locations are given in (a)). The curves are characterised

by rapid tectonic subsidence in the latest Permian to early Triassic, followed by progressively decreasing rates of subsidence throughout the Mesozoic and Cenozoic. Low magnitude, short-lived tectonic subsidence events during the Mesozoic are highlighted by arrows. Data compiled from Dixon (1989).

c. Thickness map for the Lower Jurassic of the Cleveland Basin. Contours show the thickness of the Lower Jurassic in metres. Map shows Market Weighton High (MWH), Jet Wyke (JW), Port Mulgrave (PM), Whitby East Cliff (W) and Saltwick Nab (SN). Note relatively thin Lower Jurassic at Whitby East Cliff and Saltwick Nab, compared with Jet Wyke and Port Mulgrave. After Powell (2010).

3. Stratigraphy, chemostratigraphy and mineralogy of the Cleveland Ironstone and Whitby Mudstone formations. From left to right, columns show: ammonite biozones (after Powell, 2010), formations, members and informal lithostratigraphic subdivisions (after Cox et al. 1999), generalised lithology (after Rawson and Wright 1996; key to lithologies is at the bottom of the figure), bed numbers and informal bed names (after Howarth 1962; note the break in bed numbering sequence at the base of the Whitby Mudstone Formation), % TOC (total organic carbon; after McArthur et al. 2008), weight %  $\text{SiO}_2$ , wt %  $\text{Al}_2\text{O}_3$ , wt % CaO, wt %  $\text{K}_2\text{O}$  and the ratio of  $\text{SiO}_2$  to  $\text{Al}_2\text{O}_3$  (all after, or derived from, Pye and Krinsley 1986), and the ratio of % quartz plus carbonate minerals to % quartz plus carbonate plus clay minerals (derived from Kemp et al. 2005; the width of the grey lines shows the minimum and maximum values of this ratio throughout the Whitby Mudstone Formation). Inset (bottom left) shows the mudstone lithofacies identified between the Avicula and Raisdale seams by Macquaker and Taylor (1996). Inset (bottom right) is a cross-plot of  $\text{SiO}_2$  vs. Zr (zirconium) for the Whitby Mudstone Formation (data compiled from Pye and Krinsley, 1986).

4. Faults and fractures within the Cleveland Ironstone Formation at Jet Wyke.
  - a. Looking S along the strike of W-dipping normal fault within the Cleveland Ironstone Formation. Note normal separation of the Avicula Ironstone Seam (A). Small arrows highlight the locations of erosive notches marking the positions of bed-parallel fractures in the foot- and hanging walls of the fault.
  - b. Swarms of bed-parallel fractures with calcite infill within and erosive notch in bed 33 of the Cleveland Ironstone Formation (Fig. 3).
  - c. Detailed view of a bed-parallel fracture shown in (b). Note the blocky calcite fill. Irregularities in the vein margin (arrowed) can be matched directly across the vein fill, indicating an opening-mode origin.
  - d. Surface of a sub-vertical fracture showing plumose markings and concentric arrest lines (e.g. at the upper left hand corner of the notebook).
  
5. Faults within the Jet rock and Bituminous shale at Port Mulgrave.
  - a. Lower hemisphere, equal area stereonet showing the orientations of postulated inversion-related, oblique-slip fault surfaces (great circles,  $n = 15$ ) and associated slickenline lineations (points).
  - b. Lower hemisphere, equal area stereonet showing the orientations of postulated burial-related normal fault surfaces (great circles,  $n = 5$ ) and associated slickenline lineations (points).
  - c. View south (along strike) of a W-dipping normal fault zone cutting the Jet rock. Half-arrows highlight the sense of displacement across the fault; hanging wall is to the right. Note shale gouge fill, including rotated carbonate concretion (bottom left) and drag of the relict bedding planes within the fault zone (dashed line).

- d. Dilatational jog along a fault slip surface. The slip surface and jog (beneath tip of pencil) contain calcite and bitumen fills. View towards SSE.
- 
6. Natural fractures in the Whitby Mudstone Formation at Port Mulgrave.
    - a. Lower hemisphere, equal area stereonet showing bed-parallel fractures within Bituminous shale (n = 7).
    - b. Lower hemisphere, equal area stereonet showing sub-vertical fractures within the Jet rock and Bituminous shale (n = 64).
    - c. Photograph showing the Bituminous shale cut by at least two bed-parallel fractures (at the bottom and upper-centre part of the image) and multiple sub-vertical fractures. The exposure is also cut by a gently-dipping shear surface (arrowed). View towards SSW; notebook (short dimension 12 cm) for scale.
    - d. Curve-in of bed-parallel fracture with calcite infill, towards an ENE-dipping normal fault (fault slip surface 170/47E with calcite slickenfibres 08/164). Dashed line lies immediately below the curving bedding-parallel fracture. Half arrows highlight sense of displacement across the fault, which itself contains calcite fills in dilatational jogs (e.g. between half arrows). Fault cuts Bituminous shale. View towards SSE. Pencil for scale.
    - e. Blocky calcite fill within a gently NW-dipping bed-parallel fracture. View towards SSW. Pencil for scale.
    - f. Curving-parallel relationship between two calcite-filled, sub-vertical fractures (fracture traces highlighted by arrows) and an underlying, calcite-filled, bed-parallel fracture (above tip of pencil) within Bituminous shale. View towards WSW.
- 
7. Faults and fractures within the Cement shale at Whitby east cliff.

- a. Lower hemisphere, equal area stereonet showing minor W-dipping faults (great circles;  $n = 16$ ) and through-going, sub-vertical fractures (poles to planes;  $n = 8$ ).
  - b. Cliff section showing carbonate concretion displaced in a normal sense by a W-dipping fault. Half-arrows highlight sense of displacement on fault. Note lenses of brecciated shale locally preserved within the narrow fault zone. Faults are linked by short, sub-vertical fractures containing poorly-preserved calcite fills (arrowed). View towards S. Pencil (on top of faulted carbonate concretion) for scale.
  - c. Cliff section showing intersection between calcite filled, segmented, sub-vertical opening-mode fracture (two segments are highlighted by arrows) and an array of W-dipping normal faults. View towards SSW. Pencil for scale.
8. Fractures within Bituminous shale at Saltwick Nab.
- a. Lower hemisphere, equal area stereonet showing the two principal sets of NNW-SSE ( $n = 1095$ ) WNW-ESE ( $n = 278$ ) -striking fractures (great circles).
  - b. Photograph showing dominant NNW-SSE striking sub-vertical fractures that cut Bituminous shale at Saltwick Nab. View towards W. Note the absence of bed-parallel veins at this locality. Person (ca. 1.7 m tall) for scale.
  - c. View onto the surface of a NNW-SSE striking fracture showing concentric arrest lines and faint plumose markings that radiate outwards from the centre.
  - d. Oblique photograph of the platform exposure at Saltwick Nab showing crossing (X) and abutting relationships between NNW-SSE and WNW-ESE striking fractures. W is towards the right. Compass-clinometer (long dimension 22 cm) for scale.
9. Schematic graph showing stress paths,  $\kappa$ , for sand- and clay-rich sedimentary rocks,

due to pore pressure increase (after compaction and lithification) under conditions of constant vertical stress. Stress paths assume poroelastic coupling between  $S_h$  and  $P_p$ .  $R = S_h / S_v$ ;  $\lambda = P_p / S_v$ . Initial stress ratios ( $R = 0.79$  for silty clay;  $R = 0.70$  for sandstone) result from normal compaction. Arrow illustrates the effect of disequilibrium compaction on a silty clay. Bold dashed lines separate fields of no propagation, vertical propagation and horizontal fracture propagation. After Lash and Engelder (2005).

10. Schematic graph showing stress paths,  $\kappa_f$ , for sand- and clay-rich sedimentary rocks, due to pore pressure increase under conditions of constant vertical stress in a basin undergoing fault-controlled subsidence (see text for details).  $R = S_h / S_v$ ;  $\lambda = P_p / S_v$ . Bold dashed lines separate fields of no propagation, vertical propagation and horizontal fracture propagation. Dashed lines are stress paths for which  $S_h$  acts parallel to the dip direction of the faults; solid lines are stress paths for which  $S_h$  acts parallel to fault strike. (a) Initial stress ratio ( $R$ ) is 0.70, representing the behaviour of sandstone; (b) Initial stress ratio ( $R$ ) is 0.79, representing the behaviour of silty clay. Combinations of friction angle ( $\phi$ ) and Poisson's ratio ( $\nu$ ) in (a) labelled A-F correspond to A-F in (b).

11. Graph showing the change in stress ratio,  $R$  ( $R = S_h / S_v$ ) during initial burial, exhumation and re-burial of clay-rich sediment, assuming 60 m exhumation, hydrostatic pore pressure and a friction angle ( $\phi$ ) of  $23^\circ$ . Curves calculated according to the empirical relationship between  $K_o$ , friction angle ( $\phi$ ) and over-consolidation ratio determined by Mayne and Kulhawy (1982, their equation 18) equation 18. See text for details.

12. Oblique view into the hanging wall onto an idealised elliptical normal fault surface (coloured for dip separation; red = large dip separation; dip separation is zero at the tip line

(black)). Tensile fractures predicted by an elastic dislocation model are shown in purple. Major semi-axis of the fault surface is 1075 m; minor semi-axis is 500 m. The maximum dip separation (red) is 4.65 m and lies at the centre of the fault plane. Fault dips at  $69^\circ$  in the direction shown by the single arrow. Double arrow is parallel to fault strike. The fault is embedded in an elastic half-space (not shown) (see text for discussion).

Table 1. Definition of symbols.

<b>Symbol</b>	<b>Definition</b>
$S_h$	Minimum horizontal stress
$S_v$	Vertical stress
$\sigma_1$	Maximum principal stress
$\sigma_2$	Intermediate principal stress
$\sigma_3$	Minimum principal stress
$P_p$	Pore fluid pressure
$\nu$	Poisson's ratio
$\varphi$	Friction angle
$R$	Ratio of minimum horizontal stress to vertical stress ( $S_h/S_v$ )
$\lambda$	Ratio of pore fluid pressure to vertical stress ( $P_p/S_v$ )
$K_0$	Coefficient of earth pressure at rest ( $(S_h - P_p)/(S_v - P_p)$ )
OCR	Over-consolidation ratio (Mayne and Kulhawy, 1982)

Table 2. Summary of localities.

<b>Locality</b>	<b>Location (longitude, latitude, WGS84)</b>	<b>Lithology</b>	<b>Structural setting</b>
Jet Wyke	0.7870°W, 54.5580°N to 0.7764°W, 54.5571°N	Cleveland Ironstone Formation, including well-bedded clay-, silt- and sand-rich, but TOC-poor mudstones	Cut by normal faults that post-date deposition of the Cleveland Ironstone Formation. Bed-parallel and sub-vertical fractures commonly observed.
Port Mulgrave	0.7669°W, 54.5498°N to 0.7639°W, 54.5448°N	Whitby Mudstone Formation (Jet rock and Bituminous shale), well-bedded clay-, silt- and TOC-rich mudstones	Cut by normal and oblique-slip faults that post-date deposition of the Whitby Mudstone Formation (Jet rock and Bituminous shale). Bed-parallel and sub-vertical fractures commonly observed.
Whitby East Cliff	0.5999°W, 54.4903°N to 0.6073°W, 54.4904°N	Whitby Mudstone Formation (Cement shale) poorly-bedded, bioturbated mudstones	In the footwall of the Whitby Harbour fault. Minor normal faults and sub-vertical fractures commonly observed. These structures post-date deposition of the Whitby Mudstone Formation (Cement shale)
Saltwick Nab	0.5921°W, 54.4879°N to 0.5883°W, 54.4866°N	Whitby Mudstone Formation (Jet rock and Bituminous shale), well-bedded clay-, silt- and TOC-rich mudstones	Whitby Mudstone Formation was exhumed < 60 m prior to lithification, during latest Toarcian to earliest Aalenian times. Whitby Mudstone Formation (Jet rock and Bituminous shale) cut by two dominant sets of sub-vertical fractures.

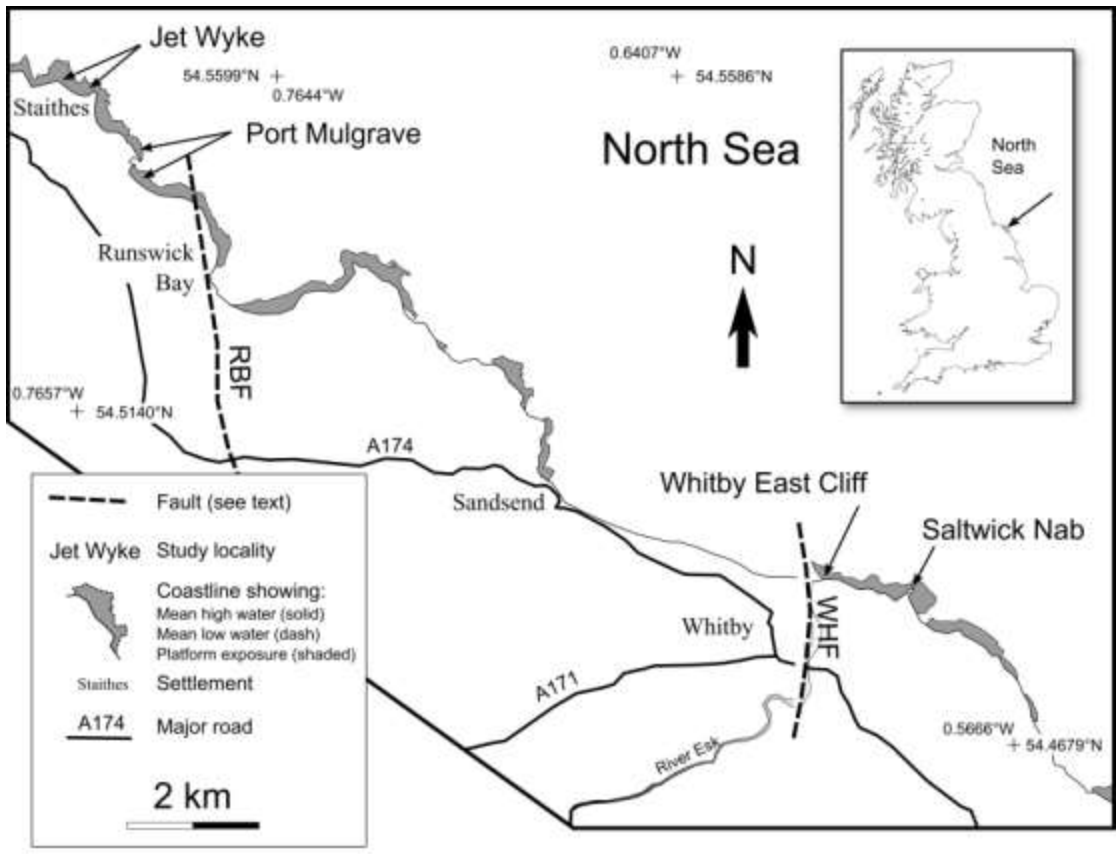


Fig. 1

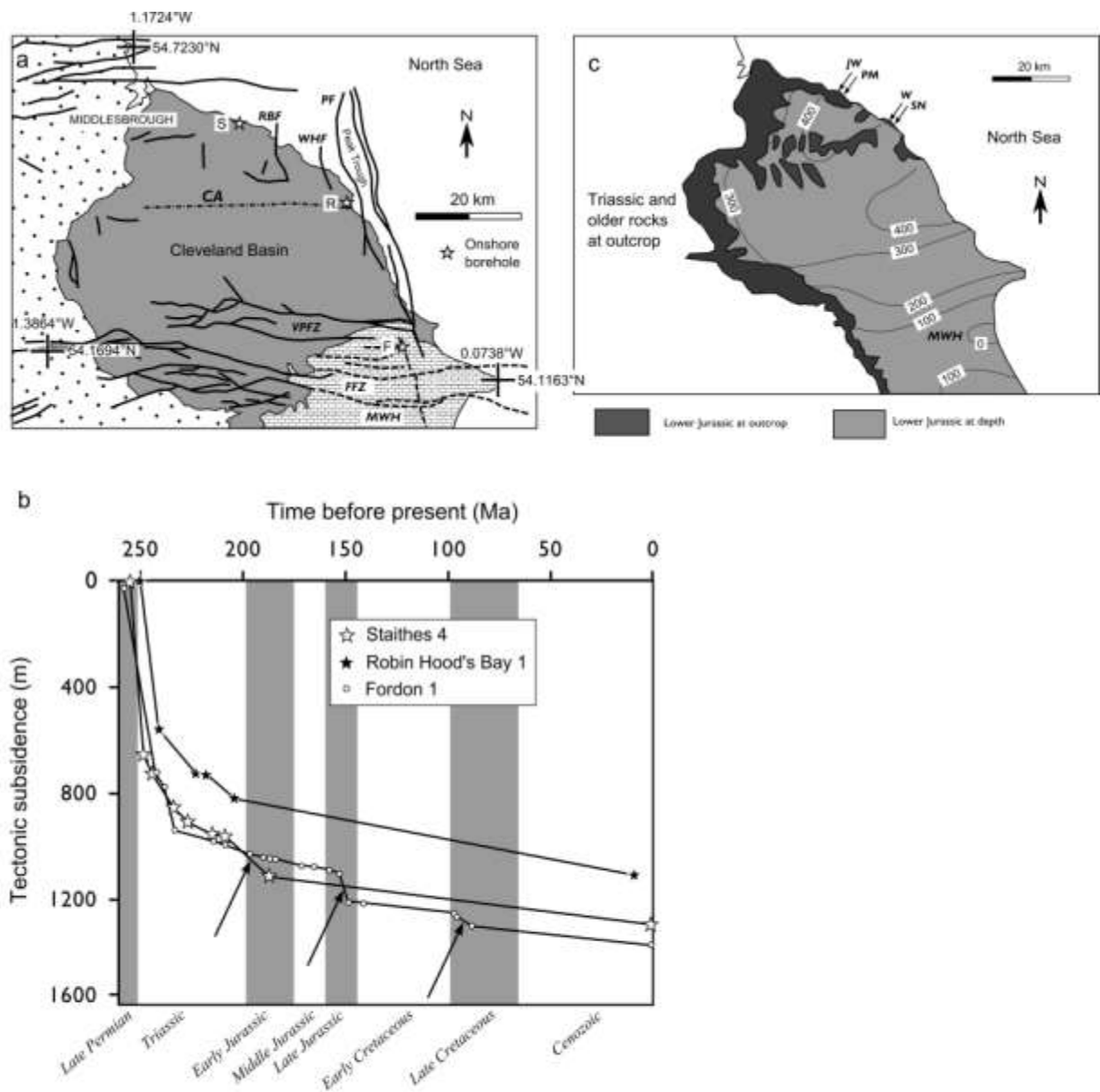
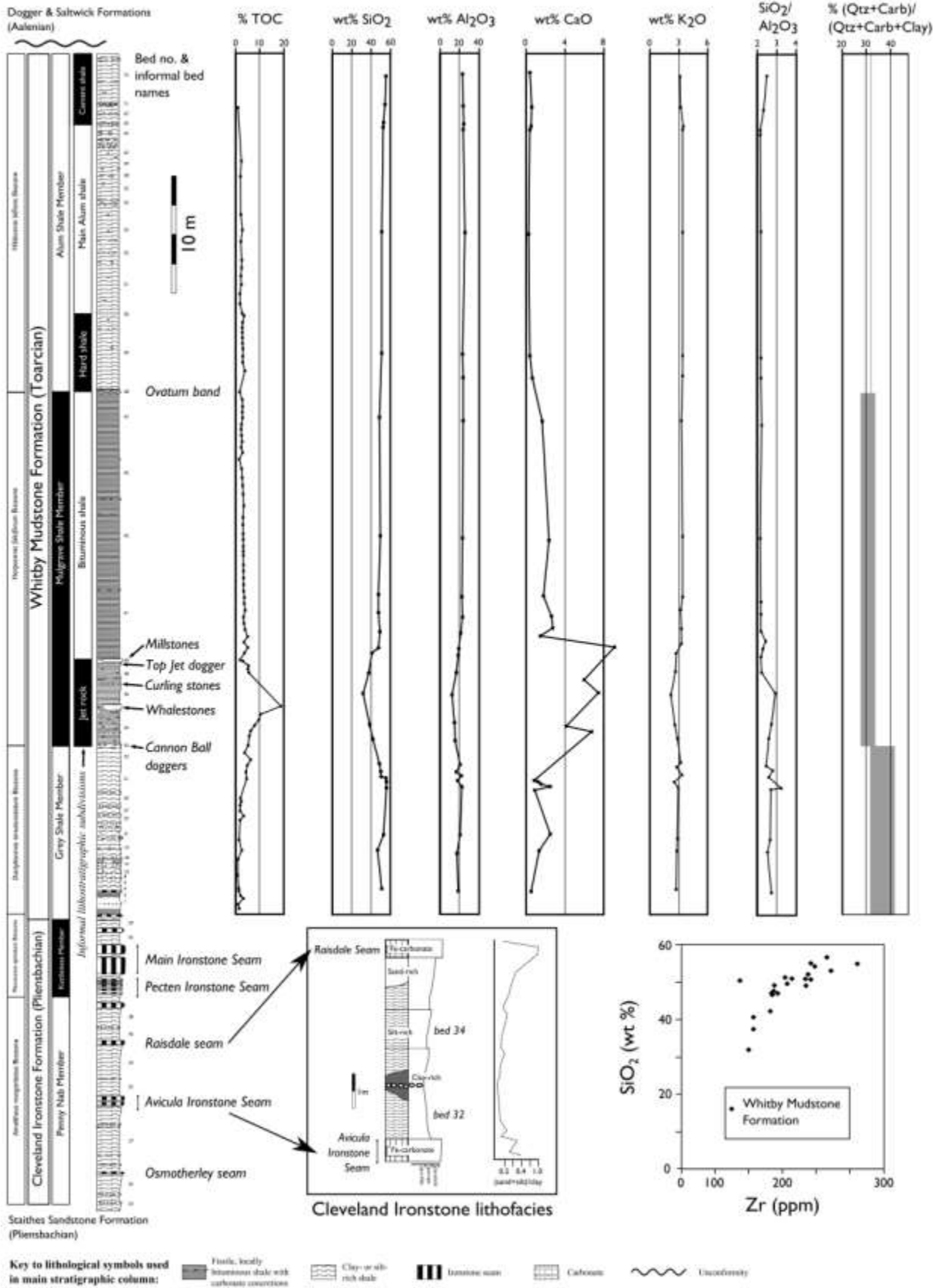


Fig. 2

# Stratigraphy

# Whole Rock Geochemistry

# Mineralogy



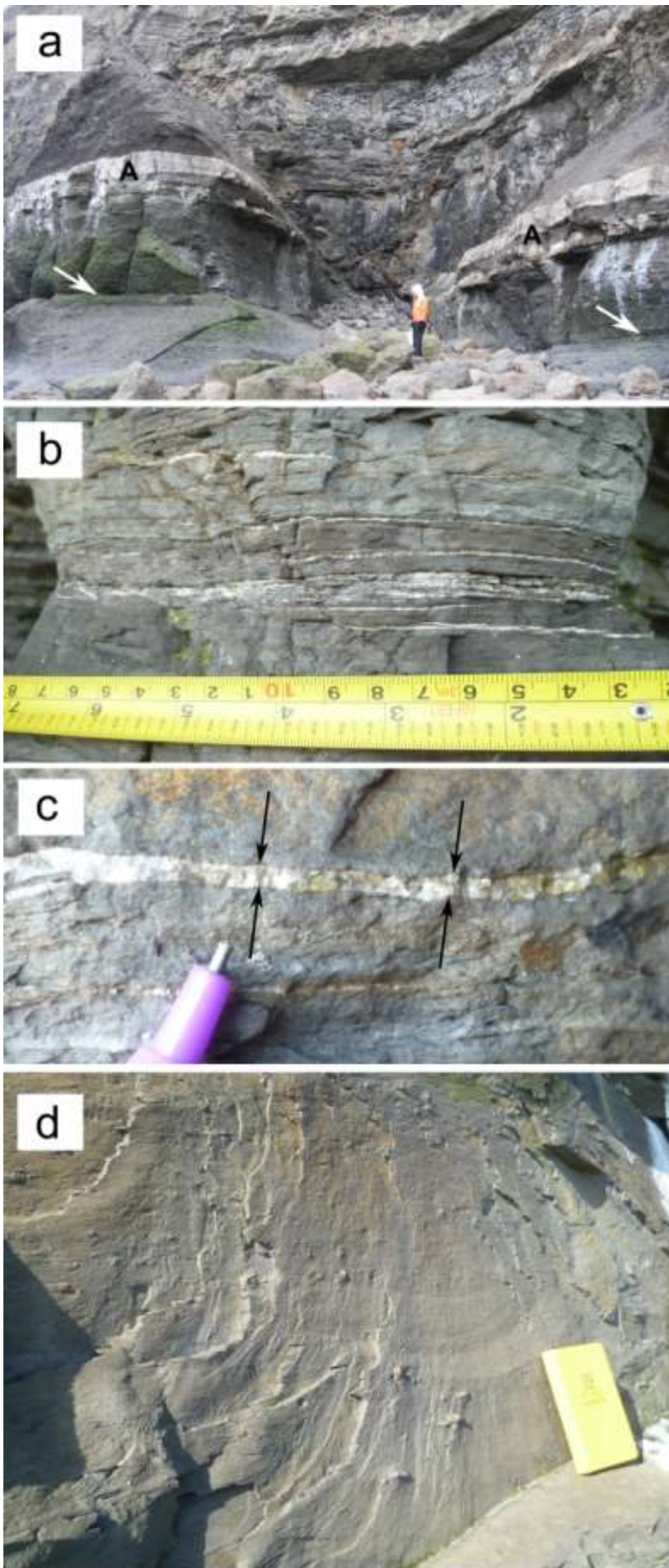


Fig. 4

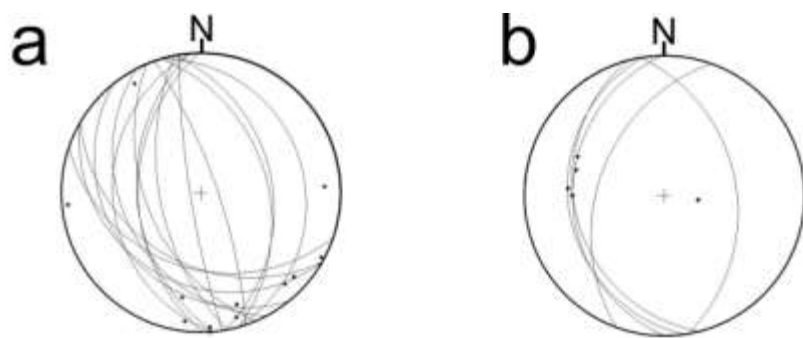


Fig. 5



Fig. 6

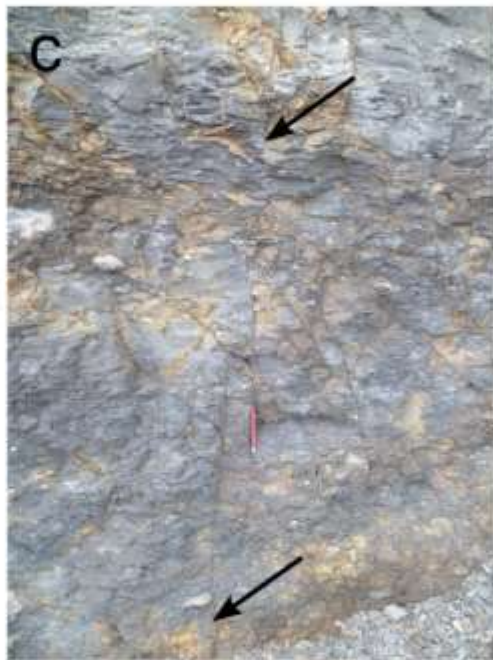
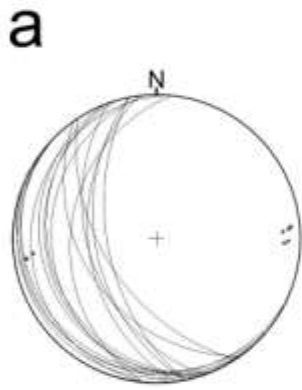


Fig. 7

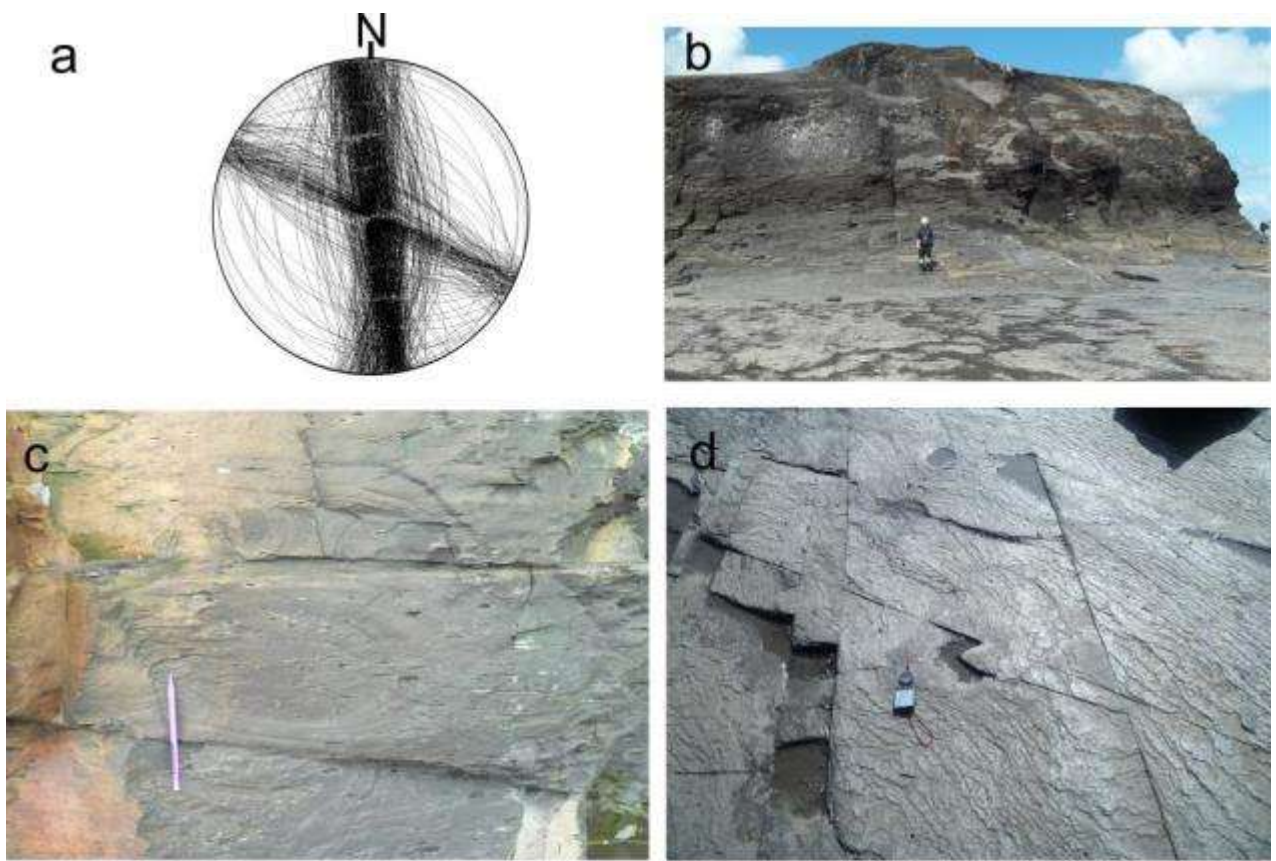


Fig. 8

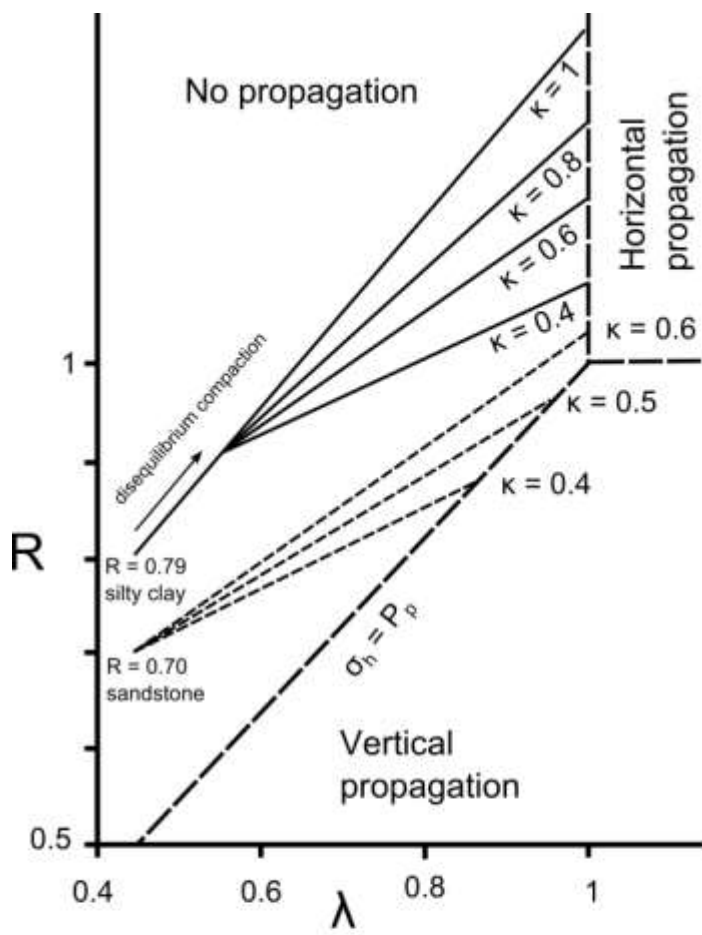


Fig. 9

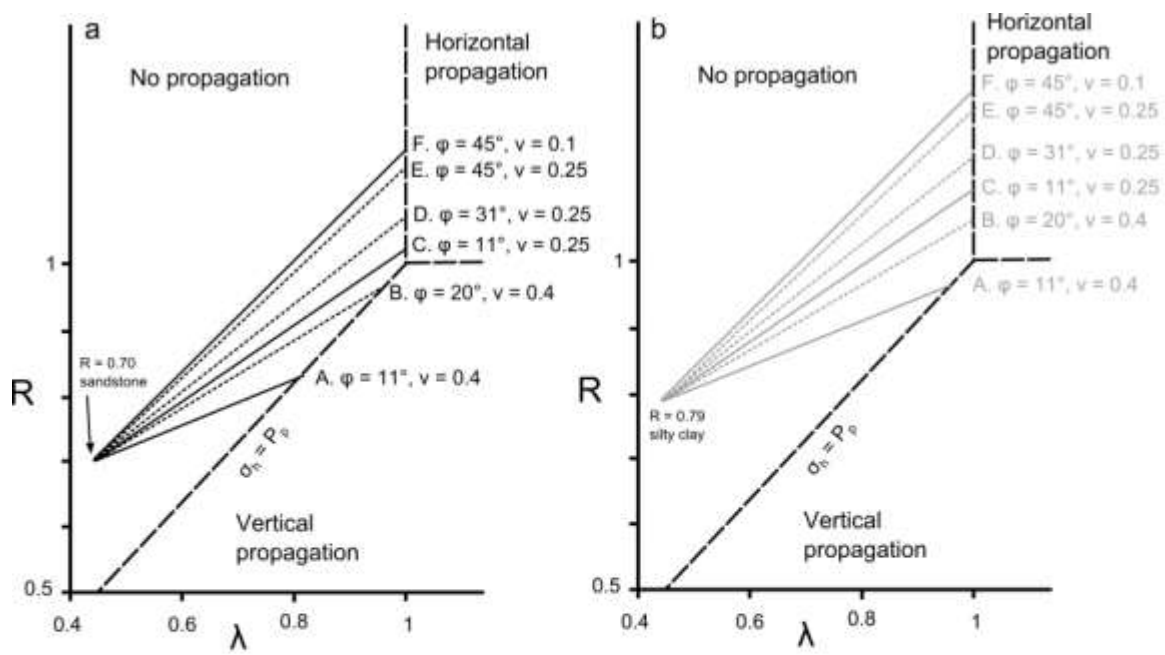


Fig. 10

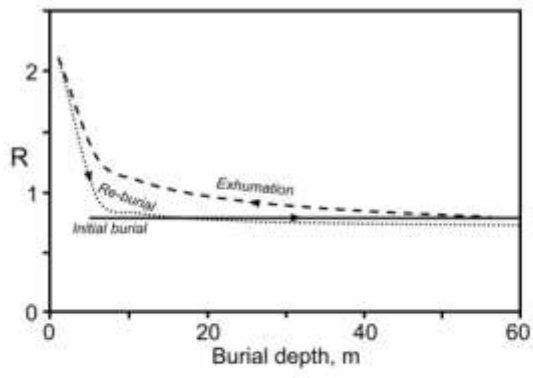


Fig. 11

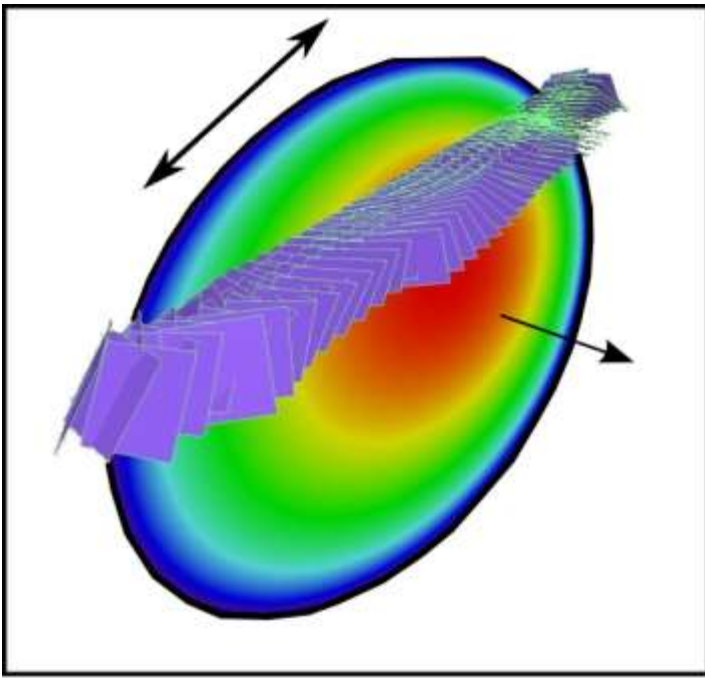


Fig. 12